4196 *Organometallics* **2009,** *28,* 4196–4209
DOI: 10.1021/om9002945

ORGANOMETALLICS
Article

Charge Delocalization in a Heterobimetallic Ferrocene−(Vinyl)Ru(CO)-Cl(P^iPr_3)$_2$ System†

Konrad Kowalski,*[,‡,§] Michael Linseis,[§] Rainer F. Winter,*[,§] Manfred Zabel,[§] Stanislav Záliš,*[,⊥] Harald Kelm,[△] Hans-Jörg Krüger,[△] Biprajit Sarkar,[▽] and Wolfgang Kaim[▽]

[‡]*Department of Organic Chemistry, Faculty of Chemistry, University of Łódź, Narutowicza 68, 90-136 Łódź, Poland,* [§]*Institut für Anorganische Chemie der Universität Regensburg, Universitätsstrasse 31, D-93040 Regensburg, Germany,* [⊥]*Heyrovský Institute of Physical Chemistry v.v.i., Academy of Science of the Czech Republic, 18223 Prague, Czech Republic,* [△]*Fachbereich Chemie der TU Kaiserslautern, Erwin-Schrödinger-Strasse, D-67663 Kaiserslautern, Germany, and* [▽]*Institut für Anorganische Chemie, Universität Stuttgart, Pfaffenwaldring, D-70569 Stuttgart, Germany*

Received April 20, 2009

Ru(CH═CHFc)Cl(CO)(P^iPr_3)$_2$ (Fc = ferrocenyl, (η^5-C_5H_4)Fe(η^5-C_5H_5)), **1**, has been prepared by hydroruthenation of ethynylferrocene and characterized by NMR, IR, ESI-MS, and Moessbauer spectroscopy and by X-ray crystallography. Complex **1** features conjoined ferrocene and (vinyl)ruthenium redox sites and undergoes two consecutive reversible oxidations. Pure samples of crystalline, monooxidized $\mathbf{1}^{\bullet+}$ have been prepared by chemical oxidation of **1** with the ferrocenium ion. Structural comparison with **1** reveals an increase of Fe−C and Fe−$Cp_{centr.}$ bond lengths and ring tilting of the Cp decks, as is typical of ferrocenium ions, but also a discernible lengthening of the Ru−C(CO) and Ru−P bonds and a shortening of the Ru−C(vinyl) bond upon oxidation. This supports the general idea of charge delocalization over both redox sites in $\mathbf{1}^{\bullet+}$. Band shifts of the charge-sensitive IR labels (ν(CO) for Ru, ν(C−H, Cp) for Fc), the rather small g-anisotropy in the ESR spectrum of $\mathbf{1}^{\bullet+}$, and the results of quantum chemical calculations indicate that in solution the positive charge partly resides on the vinyl ruthenium moiety. Comparison of IR shifts in the solid state and in solution and the quadrupole splitting in the Moessbauer spectrum of powdered $\mathbf{1}^{\bullet+}$ point to a larger extent of charge localization on the ferrocenyl site in solid samples. This is probably due to CH···F hydrogen bonding interactions between the cyclopentadienyl hydrogen atoms of the radical cations and the PF_6^- counterions. Monooxidized $\mathbf{1}^{\bullet+}$ displays low-energy electronic absorption bands at 1370 and 2150 nm. According to quantum chemical calculations, the underlying transitions are largely localized on the ferrocene part of the molecule with only little charge transfer into the vinyl ruthenium subunit. The second oxidation is more biased toward the (vinyl)ruthenium site.

Introduction

Modern studies of electronic interactions (or "communication") between metal centers in mixed-valent (MV) compounds began in the late 1960s and were spurred by the appearance of seminal papers by Allen and Hush[1,2] and Robin and Day.[3] There has been a continuing interest in that topic ever since, and a large wealth of experimental data on many varied systems have been accumulated over the years. Apart from the multitude of compounds that are structurally related to the nowadays classical inorganic Creutz−Taube ion,[4−6] there is an expanding family of organometallic complexes that are known to exhibit various degrees of electronic metal−metal interactions in their mixed-valence states.[7−21] It has

† Dedicated to Prof. Dr. Helmut Werner on the occasion of his 75th birthday

*Corresponding authors. E-mail: rainer.winter@chemie.uni-regensburg.de.

(1) Allen, G. C.; Hush, N. S. *Prog. Inorg. Chem.* **1967**, *8*, 357–389.
(2) Hush, N. S. *Prog. Inorg. Chem.* **1967**, *8*, 391–444.
(3) Robin, M. B.; Day, P. *Adv. Inorg. Chem. Radiochem.* **1967**, *10*, 247–422.
(4) Creutz, C.; Taube, H. *J. Am. Chem. Soc.* **1969**, *91*, 3988–3989.
(5) Creutz, C.; Taube, H. *J. Am. Chem. Soc.* **1973**, *95*, 1086–1094.
(6) D'Alessandro, D. M.; Keene, R. F. *Chem. Rev.* **2006**, *106*, 2270–2298.
(7) Paul, F.; Lapinte, C. *Coord. Chem. Rev.* **1998**, *178−180*, 431–509.
(8) Ceccon, A.; Santi, S.; Orian, L.; Bisello, A. *Coord. Chem. Rev.* **2004**, *248*, 683–724.
(9) Lapinte, C. *J. Organomet. Chem.* **2008**, *693*, 793–801.
(10) Wheatly, N.; Kalck, P. *Chem. Rev.* **1999**, *99*, 3379–3420.
(11) Olivier, C.; Choua, S.; Turek, P.; Touchard, D.; Rigaut, S. *Chem. Commun.* **2007**, 3100–3102.
(12) Gao, L.-B.; Kan, J.; Fan, Y.; Zhang, L.-Y.; Liu, S.-H.; Chen, Z.-N. *Inorg. Chem.* **2007**, *46*, 5651–5664.
(13) Launay, J.-P. *Chem. Soc. Rev.* **2001**, *30*, 386–397.
(14) Akita, M.; Tanaka, Y.; Naitoh, C.; Ozawa, T.; Hayashi, N.; Takeshita, M.; Inagaki, A.; Chung, M.-C. *Organometallics* **2006**, *25*, 5261–5275.
(15) Tanaka, Y.; Ozawa, T.; Inagaki, A.; Akita, M. *Dalton Trans.* **2007**, 928–933.
(16) Fernández, F. J.; Blacque, O.; Alfonso, M.; Berke, H. *Chem. Commun.* **2001**, 1266–1267.
(17) Fernández, F. J.; Venkatesan, K.; Blacque, O.; Alfonso, M.; Schmalle, H. W.; Berke, H. *Chem.—Eur. J.* **2003**, *9*, 6192–6206.
(18) Venkatesan, K.; Fox, T.; Schmalle, H. W.; Berke, H. *Organometallics* **2005**, *24*, 2834–2847.

 Published on Web 06/16/2009

been argued that knowledge on metal−metal electronic communication in MV compounds is of relevance for the fabrication of novel nanosized electronic components, devices, and conductive polymers.[22−30] Additional impetus for development in that area comes from the prospect of utilizing bimetallic redox-active systems as novel redox-switchable NLO,[31−35] electrochromic,[36−38] or luminescent materials.[39,40]

Reliable estimates of the extent of electron delocalization in MV compounds often require a combination of different experimental techniques such as electrochemistry, UV/vis/NIR, ESR, and Moessbauer spectroscopies. Each of them operates on its own inherent time scale and provides different information about the investigated MV state, and there are cases where contrasting results from techniques with different time domains have allowed one to bracket the rate of intramolecular electron transfer between the individual redox sites.[41−43] By virtue of the comproportionation constant K_c[44] electrochemical techniques such as cyclic voltammetry provide basic data about the thermodynamic stabilities of mixed-valent states with respect to their bordering isovalent ones. Comproportionation constants *per se* are, however, subject to several contributions and are thus inadequate for precisely describing the degree of electronic communication between metal centers in MV compounds.[45,46]

Most estimates of intramolecular electron-transfer efficiencies rely on the analysis of the appropriate electronic absorption band. Following Hush's theory, the electronic coupling matrix element V_{ab}, which determines the extent of charge delocalization in class II mixed-valent compounds,[3] can be determined from the so-called intervalence charge-transfer (IVCT) band that relates to the transfer of charge from the (formally) reduced to the (formally) oxidized redox site (eq 1).[1,2] While the energy $\tilde{\nu}_{max}$, the molar extinction coefficient ε_{max}, and the full width at half-height $\Delta\tilde{\nu}_{1/2}$ of the IVCT band are directly accessible from experiment, the charge-transfer distance R_{MM} presents considerable uncertainty. Thus, R_{MM} may be substantially smaller than the spatial distance between the nominal redox sites, particularly in the case of strong mixing between local orbitals of the redox-active end groups and bridge-based orbitals.[47−53] For strongly coupled, fully delocalized class III systems with no energy barrier between the adiabatic states, V_{ab} is simply half the energy at the IVCT band maximum (eq 2).

$$V_{ab} = 2.05 \times 10^{-2} \times (\varepsilon_{max}\tilde{\nu}_{max}\Delta\tilde{\nu}_{1/2})^{1/2}/R_{MM} \quad (1)$$

$$V_{ab} = \tilde{\nu}_{max}/2 \quad (2)$$

Hush's analysis may also be applied to unsymmetrical mixed-valent systems $[M-bridge-M']^{n+}$, where the two different mixed-valent isomers (valence tautomers) $[M_{ox}-bridge-M'_{red}]^{n+}$ and $[M_{red}-bridge-M'_{ox}]^{n+}$ differ in their ground-state energies and display different thermal and optical activation barriers for intramolecular electron transfer.[54−57] In that case, the energy of the optical transition equals the sum of the total reorganization energy λ and the ground-state energy difference ΔG^0 between the two valence tautomers (eq 3).[1,2] ΔG^0 may be estimated from the difference between the inherent redox potentials of the bridged sites in suitable mononuclear model systems (eq 4). Under the premises that $V_{ab} < (\lambda + \Delta G^0)$ and $|\Delta G^0| < \lambda$, the thermal barrier for IVCT from the

(19) Bruce, M. I.; Costuas, K.; Davin, T.; Ellis, B. G.; Halet, J.-F.; Lapinte, C.; Low, P. J.; Smith, M. E.; Skelton, B. W.; Toupet, L.; White, A. H. *Organometallics* **2005**, *24*, 3864–3881.
(20) Bruce, M. I.; Low, P. J.; Costuas, K.; Halet, J.-F.; Best, S. P.; Heath, G. A. *J. Am. Chem. Soc.* **2000**, *122*, 1949–1962.
(21) Bruce, M. I.; Kostuas, K.; Davin, T.; Ellis, B. G.; Halet, J.-F.; Lapinte, C.; Low, P. J.; Smith, M. E.; Skelton, B. W.; Toupet, L.; White, A. H. *Organometallics* **2005**, *24*, 3864–3881.
(22) Ward, M. *Chem. Soc. Rev.* **1995**, *24*, 121–134.
(23) Ratner, M.; Jortner, J. *Molecular Electronics*; Malden, MA, 1997.
(24) Carroll, R. L.; Gorman, C. B. *Angew. Chem., Int. Ed.* **2002**, *41*, 4378–4400.
(25) Robertson, N.; McGowan, C. A. *Chem. Soc. Rev.* **2003**, *32*, 96–103.
(26) Szafert, S.; Gladysz, J. A. *Chem. Rev.* **2006**, *106*, PR1–33.
(27) Szafert, S.; Gladysz, J. A. *Chem. Rev.* **2003**, *103*, 4175–4205.
(28) Collier, P. C.; Wong, W. E.; Belohradský, M.; Raymo, M. F.; Stoddart, F. J.; Kuekes, J. P.; Williams, S. R.; Heath, R. *Science* **1999**, *285*, 391–394.
(29) Schwab, P. F. H.; Levin, M. D.; Michl, J. *Chem. Rev.* **1999**, *99*, 1863–1934.
(30) Long, N. J.; Williams, C. K. *Angew. Chem., Int. Ed.* **2003**, *42*, 2586–2617.
(31) Long, N. J. *Angew. Chem., Int. Ed. Engl.* **1995**, *43*, 21–38.
(32) Cifuentes, M. P.; Powell, C. E.; Humphrey, M. G.; Heath, G. A.; Samoc, M.; Luther-Davies, B. *J. Phys. Chem. A* **2001**, *105*, 9625–9627.
(33) Powell, C. E.; Cifuentes, M. P.; Morrall, J. P.; Stranger, R.; Humphrey, M. G.; Samoc, M.; Luther-Davies, B.; Heath, G. A. *J. Am. Chem. Soc.* **2003**, *125*, 602–610.
(34) Powell, C. E.; Humphrey, M. G.; Cifuentes, M. P.; Morrall, J. P.; Samoc, M.; Luther-Davies, B. *J. Phys. Chem. A* **2003**, *127*, 11264–11266.
(35) Samoc, M.; Gauthier, N.; Cifuentes, M. P.; Paul, F.; Lapinte, C.; Humphrey, M. G. *Angew. Chem.* **2006**, *118*, 7536–7539.
(36) Wang, S.; Li, X.; Xun, S.; Wan, X.; Wang, Z. Y. *Macromolecules* **2006**, *39*, 7502–7507.
(37) Mortimer, R. J. *Compr. Coord. Chem.* **2004**, *9*, 581–619.
(38) Linseis, M.; Winter, R. F.; Sarkar, B.; Kaim, W.; Záliš, S. *Organometallics* **2008**, *27*, 3321–3324.
(39) Staffilani, M.; Belser, P.; De Cola, L.; Hartl, F. *Eur. J. Inorg. Chem.* **2003**, 335–339.
(40) Wong, K. M.-C.; Lam, S. C.-F.; Ko, C.-C.; Zhu, N.; Yam, V. W.-W.; Roué, S.; Lapinte, C.; Fathallah, S.; Costuas, K.; Kahlal, S.; Halet, J.-F. *Inorg. Chem.* **2003**, *42*, 7086–7097.
(41) Atwood, C. G.; Geiger, W. E. *J. Am. Chem. Soc.* **2000**, *122*, 5477–5485.
(42) Maurer, J.; Sarkar, B.; Schwederski, B.; Kaim, W.; Winter, R. F.; Záliš, S. *Organometallics* **2006**, *25*, 3701–3712.
(43) Ito, T.; Hamaguchi, T.; Nagino, H.; Yamaguchi, T.; Kido, H.; Zavarine, I. S.; Richmond, T.; Washington, J.; Kubiak, C. P. *J. Am. Chem. Soc.* **1999**, *121*, 4625–4632.
(44) Richardson, D. E.; Taube, H. *Inorg. Chem.* **1981**, *20*, 1278–1285.
(45) Kaim, W.; Lahiri, G. K. *Angew. Chem., Int. Ed.* **2007**, *44*, 1778–1795.
(46) Barrière, F.; Camire, N.; Geiger, W. E.; Mueller-Westerhoff U. T.; Sanders, R. *J. Am. Chem. Soc.* **2002**, *124*, 7262–7263.
(47) Oh, D.; Sano, M.; Boxer, S. G. *J. Am. Chem. Soc.* **1991**, *113*, 6880–6890.
(48) Dinolfo, P. H.; Lee, S. J.; Coropceanu, V.; Brédas, J.-L.; Hupp, J. T. *Inorg. Chem.* **2005**, *44*, 5789–5797.
(49) Nelsen, S. F.; Ismagilov, R. F.; Powell, D. R. *J. Am. Chem. Soc.* **1997**, *119*, 10213–10222.
(50) Nelsen, S. F.; Konradsson, A. E.; Weaver, M. N.; Tello, J. P. *J. Am. Chem. Soc.* **2003**, *125*, 12493–12501.
(51) Treynor, T. P.; Boxer, S. G. *J. Phys. Chem. A* **2004**, *108*, 1764–1778.
(52) Brunschwig, B.; Creutz, C.; Sutin, N. *Chem. Soc. Rev.* **2002**, *31*, 168–184.
(53) Lambert, C.; Amthor, S.; Schelter, J. *J. Phys. Chem. A* **2004**, *108*, 6474–6468.
(54) Santi, S.; Orian, L.; Durante, C.; Bisello, A.; Benetollo, F.; Crociani, L.; Ganis, P.; Ceccon, A. *Chem.—Eur. J.* **2007**, *13*, 1955–1968.
(55) Santi, S.; Orian, L.; Durante, C.; Bencze, E. Z.; Bisello, A.; Donoli, A.; Ceccon, A.; Benetello, F.; Crociani, L. *Chem.—Eur. J.* **2007**, *13*, 7933–7947.
(56) Caballero, A.; Espinosa, A.; Tárraga, A.; Molina, P. *J. Org. Chem.* **2007**, *72*, 6924–6937.
(57) Barlow, S. *Inorg. Chem.* **2001**, *40*, 7047–7053.

ground-state isomer can be calculated via eq 5 once V_{ab}, λ, and ΔG^0 are known.[58]

$$\tilde{\nu}_{max} = \lambda + \Delta G^0 \quad (3)$$

$$\Delta G^0 = E_{1/2}{}^{ox}(M'-\text{bridge}) - E_{1/2}{}^{ox}(M-\text{bridge}) \quad (4)$$

$$\Delta G = \lambda/4 + \Delta G^0/2 + (\Delta G^0)^2/[4(\lambda - 2V_{ab})] - V_{ab} + (V_{ab})^2/(\lambda + \Delta G^0) \quad (5)$$

Owing to the reversible nature of the ferrocene/ferrocenium redox couple, the good chemical stabilities of oxidized ferrocenium ions, and the well-developed synthetic chemistry of ferrocene, ferrocene-containing compounds are particularly attractive in this field. Thorough investigations on mixed-valent radical cations derived from homobimetallic ferrocenes and biferrocenes have significantly contributed to our present knowledge on how conformation, matrix effects, and ion pairing affect intramolecular electron-transfer rates and efficiencies.[59−68] Some ferrocenyl−π-bridge−ruthenium complexes have also been prepared and investigated with respect to intramolecular electron transfer in unsymmetrical mixed-valent systems.[56,69−78]

Here we report on heterobimetallic Ru(CH=CHFc)Cl(CO)(P^iPr_3)$_2$ (**1**, Fc = ($\eta^5C_5H_5$)Fe(η^5-C_5H_4)) and its mono- and dioxidized redox congeners (Chart 1). Comparison of the X-ray structures, the Moessbauer parameters, and the spectral positions of charge-sensitive IR labels of **1** and of $\mathbf{1}^{\bullet+}$ are used along with the ESR parameters of $\mathbf{1}^{\bullet+}$ to map their electronic structures. In particular, we address the issue of charge and spin delocalization in mixed-valent $\mathbf{1}^{\bullet+}$ and its dependence on matrix effects, i.e., the solution versus the solid state. Quantum chemical calculations aid in the rationalization of our experimental findings and provide an assignment of the electronic absorption bands of $\mathbf{1}^{n+}$ (n = 0, 1, 2).

Chart 1. Complexes 1 and $\mathbf{1}^{\bullet+}$

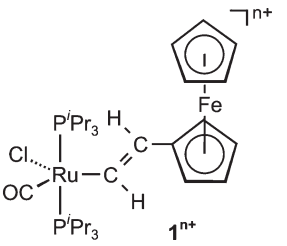

Results

Synthesis, Spectroscopic Characterization, and Solid-State Structure of 1. Complex **1** has been obtained in quantitative yield by treatment of ethynylferrocene with RuClH(CO)(P^iPr_3)$_2$ according to the well-established hydroruthenation procedure (Scheme 1).[79−85] The structure of **1** was confirmed by multinuclear NMR spectroscopy along with IR, MS, and elemental analysis. The ^{1}H NMR spectrum of **1** shows a broad doublet and a triplet of doublets for the vinyl protons at δ = 7.66 ppm (Ru−C*H*=CHFc) and at 5.54 ppm (Ru-CH=C*H*Fc). The δ values and coupling constant for the vinyl protons of **1** are in the range for similar *E*-configured (vinyl)ruthenium complexes including the closely related Ru(CH=CH−Fc)Cl(CO)(PPh_3)$_2$, which has just been reported by Wilton-Ely.[86] The ^{1}H NMR spectrum of **1** shows two virtual triplets at 4.00 and 3.98 ppm for the substituted cyclopentadienyl protons and a singlet at 4.02 ppm for the protons of the unsubstituted cyclopentadienyl ligand. In the ^{13}C NMR spectrum of **1** the Ru- and Fc-bonded vinyl carbon atoms resonate at 143.2 and 129.6 ppm with a $^2J_{P-C}$ or $^3J_{P-C}$ coupling constant of 10.7 or 3.1 Hz, respectively. The ^{31}P NMR spectrum of **1** shows a singlet at 38.6 ppm. Despite the presence of two bulky substituents, rotation around the Ru−C and Fc−C single bonds is so rapid that no broadening of the ^{31}P and ^{1}H NMR spectra is observed even at temperatures as low as 153 K. The IR spectrum of **1** shows the characteristic intense absorption band of the coordinated CO ligand at 1908 cm^{-1}, attesting to its electron-rich nature.

(58) Brunschwig, B. S.; Sutin, N. *Coord. Chem. Rev.* **1999**, *187*, 233–254.
(59) Cowan, D. O.; LeVanda, C.; Park, J.; Kauffman, F. *Acc. Chem. Res.* **1973**, *6*, 1–7.
(60) LeVanda, C.; Bechgaard, K.; Cowan, D. O. *J. Org. Chem.* **1976**, *41*, 2700–2704.
(61) Kramer, J. A.; N. Hendrickson, D. *Inorg. Chem.* **1980**, *19*, 3330–3337.
(62) Webb, R.; Hagen, P. M.; Wittebort, R. J.; Sorai, M.; Hendrickson, D. N. *Inorg. Chem.* **1992**, *31*, 1791–1801.
(63) Powers, M. J.; Meyer, T. J. *J. Am. Chem. Soc.* **1978**, *100*, 4394–4398.
(64) Amer, S. I.; Sadler, G.; Henry, P. M.; Ferguson, G.; Ruhl, B. L. *Inorg. Chem.* **1985**, *24*, 1517–1522.
(65) Lee, H.-J.; Noh, D.-Y.; Underhill, A. E.; Lee, C.-S. *J. Mater. Chem.* **1999**, *9*, 2359–2363.
(66) Dong, T.-Y.; Lee, T.-Y.; Lee, S.-H.; Lee, G.-H.; Peng, S.-M. *Organometallics* **1994**, *13*, 2337–2348.
(67) Dong, T. Y.; Huang, C.-H.; Chang, C.-K.; Hsieh, H.-S.; Peng, S.-M.; Lee, G.-H. *Organometallics* **1995**, *14*, 1776–1785.
(68) Ribou, A.-C.; Launay, J.-P.; Sachtleben, M. L.; Li, H.; Spangler, C. W. *Inorg. Chem.* **1996**, *35*, 3735–3740.
(69) Sato, M.; Shintate, H.; Kawata, Y.; Sekino, M.; Katada, M.; Kawata, S. *Organometallics* **1994**, *13*, 1956–1962.
(70) Colbert, M. C. B.; Lewis, J.; Long, N. J.; Raithby, P. R.; White, A. J. P.; Williams, D. J. *J. Chem. Soc., Dalton Trans.* **1997**, 99–104.
(71) Jones, N. D.; Wolf, M. O.; Giaquinta, D. M. *Organometallics* **1997**, *16*, 1352–1354.
(72) Bruce, M. I.; Low, P. J.; Hartl, F.; Humphrey, P. A.; de Montigny, F.; Jevric, M.; Lapinte, C.; Perkins, G. J.; Roberts, R. L.; Skelton, B. W.; White, A. H. *Organometallics* **2005**, *24*, 5241–5255.
(73) Yuan, P.; Liu, S. H.; Xiong, W.; Yin, J.; Yu, G.-a.; Sung, H. Y.; Williams, I. D.; Jia, G. *Organometallics* **2005**, *24*, 1452–1457.
(74) Dowling, N.; Henry, P. M. *Inorg. Chem.* **1982**, *21*, 4088–4095.
(75) Dowling, N.; Henry, P. M.; Lewis, N. A.; Taube, H. *Inorg. Chem.* **1981**, *20*, 2345–2348.
(76) Liu, T.-Y.; Chen, Y. J.; Tai, C.-C.; Kwan, K. S. *Inorg. Chem.* **1999**, *38*, 674–679.
(77) Chen, Y. J.; Kao, C.-H.; Lin, S. J.; Tai, C.-C.; Kwan, K. S. *Inorg. Chem.* **2000**, *39*, 189–194.
(78) Lohan, M.; Ecorchard, P.; Rüffer, T.; Justaud, F.; Lapinte, C.; Lang, H. *Organometallics* **2009**, *28*, 1878–1890.
(79) Torres, M. R.; Vegas, A.; Santos, A. *J. Organomet. Chem.* **1986**, *309*, 169–177.
(80) Hill, A. F. In *Comprehensive Organometallic Chemistry II*; Shriver, D. E.; Bruce, M. I., Eds.; Pergamon: Oxford, 1995; Vol. 7, pp 399−411.
(81) Esteruelas, M. A.; Werner, H. *J. Organomet. Chem.* **1986**, *303*, 221–231.
(82) Werner, H.; Esteruelas, M. A.; Otto, H. *Organometallics* **1986**, *5*, 2295.
(83) Werner, H.; Meyer, U.; Peters, K.; von Schnering, H. G. *Chem. Ber.* **1989**, *122*, 2089–2107.
(84) Santos, A.; López, J.; Montoya, J.; Noheda, P.; Romero, A.; Echavarren, A. M. *Organometallics* **1994**, *13*, 3605–3615.
(85) Marchenko, A. V.; Gérard, H.; Eisenstein, O.; Caulton, K. G. *New J. Chem.* **2001**, *25*, 1244–1255.
(86) Macgregor, M. J.; Hogarth, G.; Thompson, A. L.; Wilton-Ely, J. D. E. T. *Organometallics* **2009**, *28*, 197–208.

Scheme 1. Synthesis of Complexes 1 and $1^{\bullet+}$

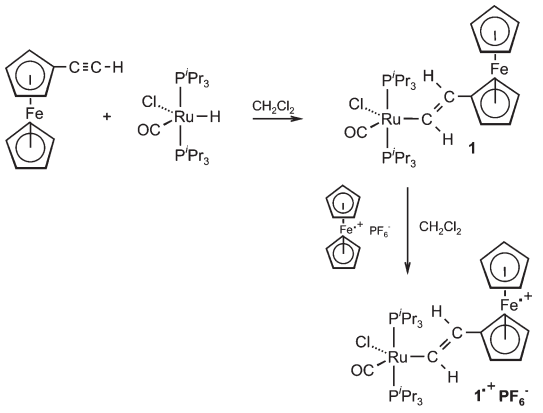

The identity of **1** and its structural features were finally established by X-ray crystallography. Crystals that were suitable for X-ray analysis were obtained by cooling a solution of **1** in a $CHCl_3/CH_3OH$ mixture in the freezer. Unexpectedly this procedure yielded two forms of crystals of green or purple color. Both these polymorphs are chloroform monosolvates. The unit cell of the green polymorph of **1**×**CHCl$_3$** contains two molecules of **1** and two molecules of $CHCl_3$, whereas there are four molecules of **1** and four molecules of $CHCl_3$ in the unit cell of the purple polymorph. We also succeeded in obtaining X-ray quality crystals of solvent-free **1** by cooling a saturated hot *n*-hexane solution. The molecular structures of **1** in these different crystals are shown in Figures 1 and S1 and S3 of the Supporting Information, while their chief metrical parameters are compiled in Table 1.

In each of the three analyzed crystalline forms complex **1** adopts a slightly different conformation. Such conformational polymorphism[87] indicates high torsional flexibility and is consistent with the free rotation of the Fc (Fc = $(\eta^5\text{-}C_5H_4)Fe(\eta^5\text{-}C_5H_5)$) and $RuCl(CO)(P^iPr_3)_2$ entities around the Fc−C and Ru−C bonds, as is indicated by our variable-temperature NMR experiments. The most general structural features of **1** present in all three analyzed crystals are the distorted square-pyramidal coordination geometry of the Ru atom, the *E* arrangement of the ferrocenyl and $RuCl(CO)(P^iPr_3)_2$ substituents at the C=C double bond, and the archetypical sandwich structure of the capping ferrocenyl entity. The four atoms P(1), P(2), Cl(1), and C(1) at the pyramid base form an approximate plane, whereas the ruthenium atom is slightly displaced out of this plane toward the apical vinyl substituent, as is routinely observed for such complexes.[82,88−93] The distortion from ideal square-pyramidal coordination around the Ru atom is also reflected by compression of the P(1)−Ru(1)−P(2) angle toward the vacant coordination site to 168.37(4)° (**1**×**CHCl$_3$**, green polymorph), 170.31(3)° (**1**×**CHCl$_3$**, purple polymorph), or 170.05(2)° (solvent-free crystal). The Ru−C and C=C bond lengths in **1** are within a range of 1.819(4) to 1.842(5) Å and 1.325(5) to 1.342(5) Å, respectively, while the =C−C bond length is uniformly at 1.464 Å. The planes formed by Ru(1) and C(20), C(21) of the vinyl substituent and the substituted cyclopentadienyl ring deviate from coplanarity and form angles of 19.1° in (**1**×**CHCl$_3$**, green polymorph), 22.2° (**1**×**CHCl$_3$**, purple polymorph), and 19.5° (solvent-free crystal). The vinyl ligand resides in the plane defined by the Ru(1), Cl(1), and C(1) atoms, as shown by the torsional angle Cl(1)−Ru(1)−C(20)−C(21) of 176.8(4)° (green polymorph of **1**×**CHCl$_3$**), −175.9(4)° (purple polymorph of **1**×**CHCl$_3$**), or −165.7(2)° (solvent-free crystal). The iron atom exhibits slightly longer distances to the centroid of the substituted cyclopentadienyl ligand in the chloroform solvates but equal distances to the centroids of both rings in the solvent-free form. In all analyzed crystals the ferrocenyl moiety adopts a geometry intermediate between staggered and eclipsed. The average $C(Cp_{sub})-Cp_{sub,Centr}-Cp_{Centr}-C(Cp)$ angles range from 14.6° to 4.4°. The Cp and Cp_{sub} planes are slightly inclined toward each other (see Table 1).

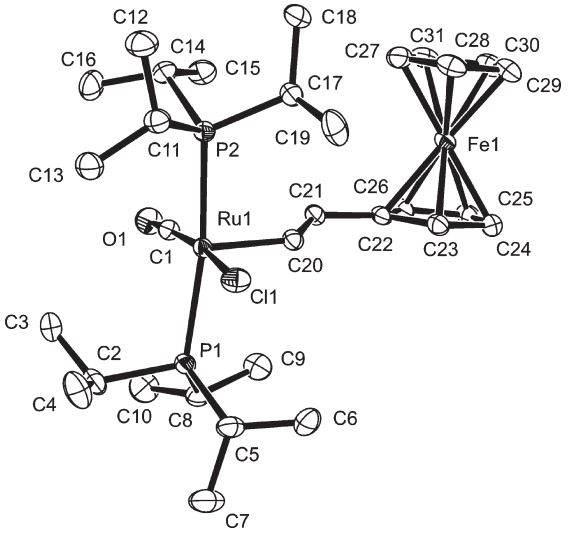

Figure 1. ORTEP view of complex **1** (solvent-free crystal). Hydrogen atoms are omitted for clarity. Ellipsoids are drawn at a 50% probability level. Selected bond lengths (Å) and angles (deg): Ru−C1, 1.820(2); Ru−Cl, 2.4380(5); Ru−C20, 1.996(2); Ru−P1, 2.4106(5); Ru−P2, 2.3947(5); C20−C21, 1.339(3); C21−C22, 1.463(3); P1−Ru−P2, 170.05(2); Cl−Ru−C1, 171.73(6); Ru−C1−O1, 178.3(2); Cl−Ru−C20, 98.38(5); Ru−C20−C21, 134.8(2); C20−C21−C22, 123.6(2).

The chloroform molecules present in the crystal lattices of the polymorphs of **1**×**CHCl$_3$** engage in various hydrogen-bonding interactions with the complex molecules, as shown in Figures S2 and S4 of the Supporting Information. First, there are contacts of 2.647 Å (green form) or 2.598 Å (purple form) between the chloroform hydrogen atom H(32) and the ruthenium-bonded chloro ligand Cl(1). Second, one proton on one ^{i}Pr substituent interacts weakly with one chlorine atom of the chloroform solvate. In the green polymorph there are additional interactions of this same chlorine atom with one C−H on ferrocene, whereas in the purple polymorph the ferrocene C−H interacts with the Ru−Cl atom instead.

Electrochemistry of 1 and Spectroscopic Characterization of $1^{\bullet+}$. In voltammetric experiments (CH_2Cl_2/NBu_4PF_6

(87) Nangia, A. *Acc. Chem. Res.* **2008**, *41*, 595–604.
(88) Huang, D.; Streib, W. E.; Bollinger, J. C.; Caulton, K. G.; Winter, R. F.; Scheiring, T. *J. Am. Chem. Soc.* **1999**, *121*, 8087–8097.
(89) Jung, S.; Ilg, K.; Brandt, C. D.; Wolf, J.; Werner, H. *Eur. J. Inorg. Chem.* **2004**, 469–480.
(90) Alcock, N. W.; Cartwright, J.; Hill, A. F.; Marcellin, M.; Rawles, H. M. *J. Chem. Soc., Chem. Commun.* **1995**, 369–370.
(91) Maruyama, Y.; Yamamura, K.; Sagawa, T.; Katayama, H.; Ozawa, F. *Organometallics* **2000**, *19*, 1308–1318.
(92) Maurer, J.; Linseis, M.; Sarkar, B.; Schwerderski, B.; Niemeyer, M.; Kaim, W.; Záliš, S.; Anson, C.; Zabel, M.; Winter, R. F. *J. Am. Chem. Soc.* **2008**, *130*, 259–268.
(93) Pichlmaier, M.; Winter, R. F.; Zabel, M.; Záliš, S. *J. Am. Chem. Soc.* **2009**, *131*, 4892–4903.

Table 1. Selected Bonding Parameters (*d* in Å, angles in deg) of 1, the two polymorphs of 1×CHCl$_3$, 1$^{\bullet+}$PF$_6^-$, and 1$^{\bullet+}$PF$_6^-$×CHCl$_3$

	1	**1×CHCl$_3$** (green polymorph)	**1×CHCl$_3$** (purple polymorph)	**1$^{\bullet+}$PF$_6^-$**	**1$^{\bullet+}$PF$_6^-$×CHCl$_3$**
Ru−Cl	2.4380(5)	2.4291(11)	2.4337(10)	2.4305(10)	2.4041(13)
Ru−P	2.4106(5), 2.3947(5)	2.4022(11), 2.4021(11)	2.4058(9), 2.4048(9)	2.4260(10), 2.4252(10)	2.4156(10), 2.4112(11)
Ru−C(CO)	1.820(2)	1.842(5)	1.819(4)	1.851(4)	1.846(6)
Ru−C(vinyl)	1.9958(19)	2.007(4)	2.005(4)	1.955(4)	1.938(3)
C=C	1.339(3)	1.325(5)	1.342(5)	1.354(5)	1.328(7)
=C−C(Fe)	1.463(3)	1.464(6)	1.464(5)	1.458(5)	1.459(7)
Fe−C(Cp$_{sub,average}$)	2.051	2.050	2.049	2.087	2.065
Fe−C(Cp$_{unsub,average}$)	2.048	2.029	2.044	2.091	2.070
Fe−Cp$_{sub,centr.}$	1.653	1.658	1.656	1.699	1.690
Fe−Cp$_{unsub,centr.}$	1.654	1.647	1.651	1.712	1.699
P−Ru−P	170.05(2)	168.37(4)	170.31(3)	167.86(4)	166.83(4)
OC−Ru-Cl	171.73(6)	170.5(2)	175.23(12)	168.16(13)	177.2(7)
Ru−C=C	134.8(2)	135.2(3)	134.7(3)	134.2(3)	138.3(4)
C=C−C	123.6(2)	125.1(4)	123.4(3)	124.8(3)	122.3(5)
Ru−C=C−C	179.4(2)	−166.2(3)	179.7(3)	−166.2(3)	−167.5(3)
RuVinyl vs Cp$_{sub}$[a]	8.9	16.7	17.9	11.2	10.2
interplanar angle (Cp)[b]	1.4	3.1	2.4	12.9	8.1
Cp$_{sub}$−Fe−Cp$_{unsub}$[c]	0.3	178.2	178.3	172.7	174.7

[a]Angle between the best plane through the atoms Fe, Cl, C(CO), and C20, C21 of the vinyl group and the plane of the substituted cyclopentadienyl ring. [b]Angle between the best cyclopentadienyl ring planes. [c]Angle between the centroids of each cyclopentadienyl ring and the iron atom.

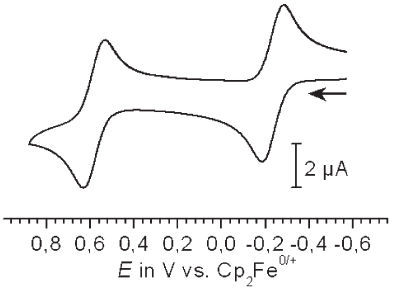

Figure 2. Voltammogram of **1** (NBu_4PF_6, 0.1 M, CH_2Cl_2, rt) at v = 0.1 V/s.

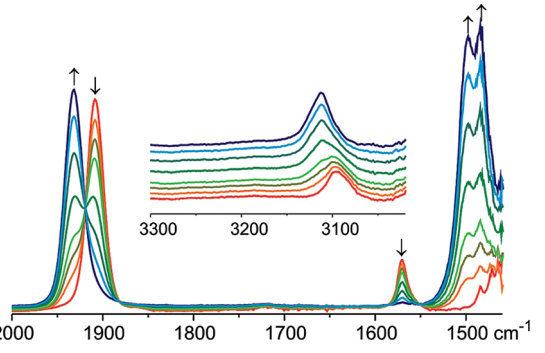

Figure 3. IR spectroscopic changes in the mid-IR upon the first oxidation of complex **1** (1,2-$C_2H_4Cl_2$/NBu_4PF_6) at r.t.

0.1 M) complex **1** undergoes two consecutive one-electron oxidations at half-wave potentials of −0.235 and 0.580 V as measured against the internal ferrocene/ferrocenium redox standard (Figure 2). Both waves show all attributes of uncomplicated Nernstian-type redox couples such as identical peak-to-peak separations, half-widths, and peak current functions as the internal ferrocene standard. The apparent stability of **1** in three oxidation states and the presence of charge-sensitive spectroscopic labels on the ruthenium (ν(CO)) and ferrocene (ν(CH, Cp))[94] sites prompted us to study the spectroscopic changes accompanying stepwise oxidation. These studies were performed inside an optically transparent thin-layer electrolysis (OTTLE) cell in the 1,2-$C_2H_4Cl_2$/NBu_4PF_6 supporting electrolyte. The most characteristic changes in the IR spectra upon the first oxidation are the ν(CO) shift of the ruthenium-bonded carbonyl ligand from 1908 to 1932 cm^{-1} and the replacement of the medium intense 1571 cm^{-1} absorption of the vinyl substituent by much stronger absorptions at 1498 and 1485 cm^{-1} (Figure 3 and Table 2). Also of note is the shift of the cyclopentadienyl CH stretch from 3096 to 3110 cm^{-1} (see inset of Figure 3). There are clear isosbestic points, and neutral **1** was obtained in quantitative spectroscopic yield when the solution was reduced back after the first oxidation had gone to completion. The fully reversible behavior of the second oxidation in voltammetric studies is, however, not retained on the longer time scale of electrolysis inside our OTTLE cell. After the initial rise of the bands of the dioxidized **1**$^{2+}$ dication at 3120 (ν(CH), Fc), 2004 (ν(CO), RuCO), and 1572 (probably ν(C=C)) a secondary species, presumably $RuCl_2(CO)(P^iPr_3)_2$, with ν(CO) = 1968 cm^{-1} started to grow in before consumption of the **1**$^{\bullet+}$ radical cation had gone to completion (Figure 4). During the final stages of the electrolysis or when the solution was left in the cell after full oxidation of **1**$^{\bullet+}$, the band intensities of all absorptions associated with **1**$^{2+}$ decreased at the expense of this secondary product (Figure S5 of the Supporting Information). Back-reduction to the radical cation caused the remaining absorptions of fully oxidized **1**$^{2+}$ to vanish while the bands of **1**$^{\bullet+}$ grew in (Figure S6 of the Supporting Information). This lends further credibility to our assignment of the 3120 and 2004 cm^{-1} absorptions to dioxidized **1**$^{2+}$. When these measurements were conducted on a more extended energy range of up to 8000 cm^{-1}, two additional broad absorptions at 7340 and 4640 cm^{-1} were found to be associated with singly oxidized **1**$^{\bullet+}$ (see Figure S7 of the Supporting Information). These bands originate from low-energy electronic excitations and were also observed in our UV/vis/NIR studies.

The electronic spectrum of neutral **1** is rather unremarkable, featuring an intense $\pi \rightarrow \pi^*$ band at 300 nm and a weaker absorption at 381 nm, which are associated with the

(94) Fritz, H. P. Infrared and Raman Spectral Studies of π-Complexes Formed Between Metals and C_nH_n Rings. In *Advances in Organometallic Chemistry*; Stone, F. G. A., West, R., Eds.; Academic Press: New York, 1964; Vol. 1, pp 239−316.

Table 2. Spectroscopic Data of 1 and Its Oxidation Products

compound	IR bands [energy in cm^{-1}][a]	UV/vis/NIR [λ_{max} in nm/ energy in cm^{-1} (ε_{max})][b]
1	ν(CH) = 3096, ν(CO) = 1908, ν(C=C) = 1571	300/33 380 (17 000), 381/26 242 (2340), 455/21 975 (525), 529/18 905 (360)
$\mathbf{1}^{\bullet+}$	ν(CH) = 3110, ν(CO) = 1932, ν(C=C) = 1498, 1485, ν(Ru−C) + δ(Ru−C−C) = 555, electronic bands at 7340, 4640	278/36 000 (11 500), 364/27 435 (980), 415/24 070 (3150), 504/19 840 (3320), 556/17 890 (5000), 1371/7290 (2700), 2150/4650 (710)
$\mathbf{1}^{2+}$[c]	ν(CH) = 3120, ν(CO) = 2004, ν(C=C) = 1572	418/23 920 (~13 500), 540/18 520(sh)

[a] In 1,2-$C_2H_4Cl_2$/NBu_4PF_6. [b] Deconvoluted data in CH_2Cl_2. [c] Generated by electrolysis in 1,2-$C_2H_4Cl_2$/NBu_4PF_6 (0.2 M). Partial decomposition to presumably $RuCl_2(CO)(P^iPr_3)_2$ occurred during these measurements such that the ε value is a lower limit.

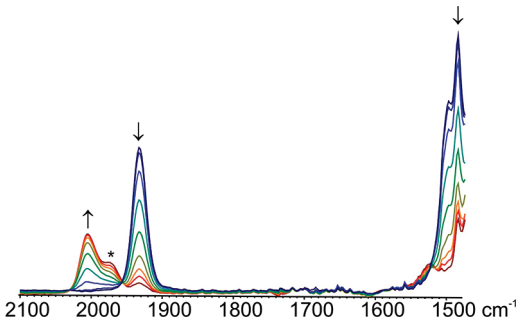

Figure 4. IR spectroscopic changes in the mid-IR upon the second oxidation of complex **1** (1,2-$C_2H_4Cl_2$/NBu_4PF_6) at rt. The star symbol designates the decomposition product.

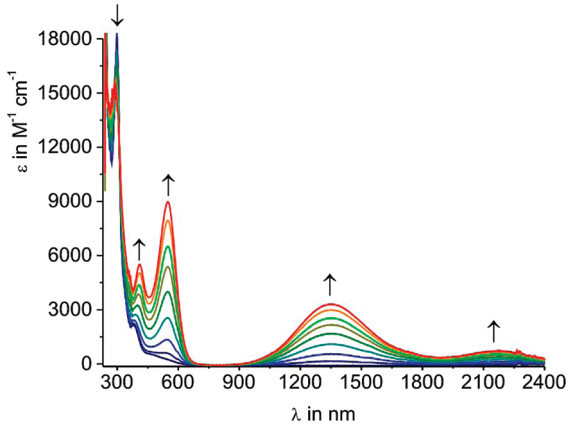

Figure 5. Spectroscopic changes during the first oxidation of **1** (1,2-$C_2H_4Cl_2$, NBu_4PF_6, rt).

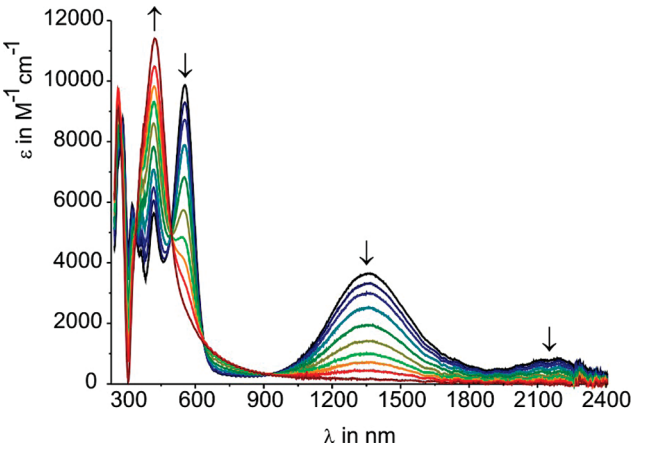

Figure 6. Spectroscopic changes during the oxidation of $\mathbf{1}^{\bullet+}$ to $\mathbf{1}^{2+}$ (1,2-$C_2H_4Cl_2$, NBu_4PF_6, rt).

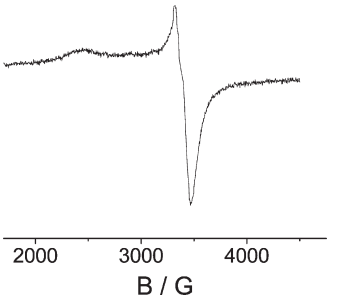

Figure 7. ESR spectrum of electrogenerated $\mathbf{1}^{\bullet+}$ in CH_2Cl_2/NBu_4PF_6 at T = 110 K.

ferrocene and the (vinyl)ruthenium chromophore. Two overlapping bands at lower energy are associated with Fe → (vinyl)ruthenium charge-transfer and a d/d-type transition within the ferrocene nucleus (*vide infra*). One-electron oxidation to $\mathbf{1}^{\bullet+}$ in the 1,2-$C_2H_4Cl_2$/NBu_4PF_6 electrolyte caused the growth of new absorptions at 281, 413, 550, 1349, and 2164 nm (Figure 5), the latter two of which correspond to the NIR bands that were also observed in our IR measurements. Partial decomposition of higher oxidized $\mathbf{1}^{2+}$ was also encountered in UV/vis/NIR spectroelectrochemistry. New bands at 418 and 540(sh) nm that developed upon the second oxidation process (Figure 6) can nevertheless be assigned to $\mathbf{1}^{2+}$, as they decreased in intensity when the fully oxidized solution was left undisturbed or, along with partial recovery of the $\mathbf{1}^{\bullet+}$ bands, when the solution was reduced at a potential sufficiently negative of the $\mathbf{1}^{2+/+}$ wave. The spectroscopic yield of $\mathbf{1}^{\bullet+}$ after a full $\mathbf{1}^{\bullet+} \rightarrow \mathbf{1}^{2+} \rightarrow \mathbf{1}^{\bullet+}$ cycle was typically in the range of 60% to 65%. ESR spectroscopy of $\mathbf{1}^{\bullet+}$ that was electrogenerated in an ESR tube gave no signal at room temperature but an intense axial signal with $g_{\parallel}$ = 2.80 and $g_{\perp}$ = 1.984 when frozen in an CH_2Cl_2 matrix at 110 K (Figure 7).

Synthesis, Structure, and Spectroscopy of Oxidized $\mathbf{1}^{\bullet+}\mathbf{PF_6^-}$. The low first oxidation potential of −235 mV against the Fc/Fc^+ couple and the good stability of $\mathbf{1}^{\bullet+}$ on even the extended time scale of bulk electrolysis suggested that this radical cation constitutes a viable synthetic target. Thus, $\mathbf{1}^{\bullet+}\mathbf{PF_6^-}$ was obtained in nearly quantitative yield as a violet, air-stable powder when a solution of **1** in CH_2Cl_2 was treated with $Fc^+PF_6^-$ at room temperature (Scheme 1). As expected, the ^1H NMR spectrum of paramagnetic $\mathbf{1}^{\bullet+}\mathbf{PF_6^-}$ shows only broad signals (see Experimental Section). Solution IR, UV/vis/NIR, and ESR spectra of pure $\mathbf{1}^{\bullet+}\mathbf{PF_6^-}$ are identical to those obtained for electrogenerated $\mathbf{1}^{\bullet+}$.

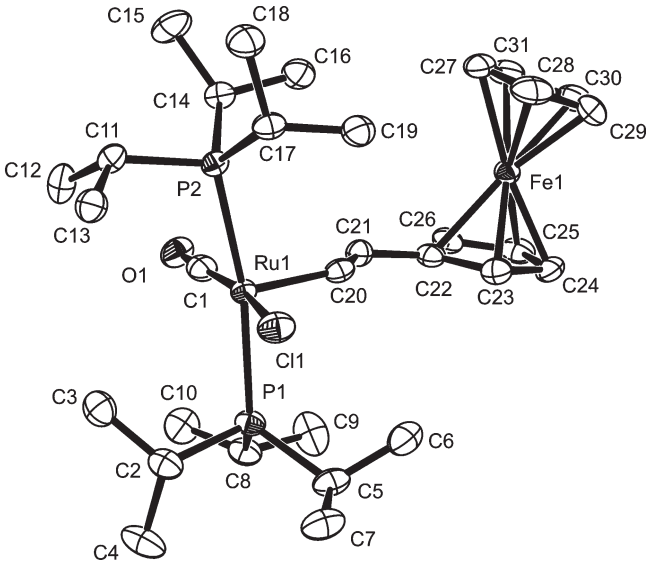

Figure 8. ORTEP view of $\mathbf{1}^{\bullet+}$ (solvent-free crystal). Hydrogen atoms are omitted for clarity. Ellipsoids are drawn at a 50% probability level. Selected bond lengths (Å) and angles (deg): Ru−C1, 1.851(4); Ru−Cl1, 2.4305(10); Ru−C20, 1.955(4); Ru−P1, 2.4260(10); Ru−P2, 2.4252(10); C20−C21, 1.354(5); C21−C22, 1.458(5); P1−Ru−P2, 167.86(4); Cl1−Ru−C1, 168.16(13); Ru−C1−O1, 176.2(4); Cl1−Ru−C20, 102.50(9); Ru−C20−C21, 134.2(3); C20−C21−C22, 124.8(3).

X-ray quality crystals of $\mathbf{1}^{\bullet+}\mathbf{PF_6^-}$ and of the monosolvate $\mathbf{1}^{\bullet+}\times\mathbf{CHCl_3}\ \mathbf{PF_6^-}$ were grown by layering concentrated solutions in dichloromethane or chloroform with *n*-hexane. The molecular structure of the cationic part of solvent-free $\mathbf{1}^{\bullet+}\mathbf{PF_6^-}$ is shown in Figure 8, while that of $\mathbf{1}^{\bullet+}\times\mathbf{CHCl_3PF_6^-}$ is shown in Figure S8 of the Supporting Information. Pertinent metrical parameters are collected in Table 1 and compared to those of the neutral congener. Both solid-state structures feature complex cations and anions that are associated by three or four CH···F hydrogen bonds between cyclopentadienyl C−H and fluorine atoms of the PF_6^- counterions. These contacts range from 2.371 to 2.609 Å in the solvent-free crystal and from 2.473 to 2.632 Å in the chloroform solvate and fixate the PF_6^- counterions, thus preventing rotational disorder, which is an often-encountered problem in PF_6^- salts lacking such interactions. Additional contacts of 2.346 and 2.562 Å between two fluorine atoms and H−C of the cocrystallized chloroform exist in the monosolvate. Packing diagrams are given in Figures S9 and S10 of the Supporting Information. The chief structural features of neutral **1** such as the square-planar coordination of ruthenium and the rough coplanarity of the substituted ferrocenyl ring with the Ru(CH=CH)Cl(CO) unit are fully retained in the oxidized form. There are nevertheless some subtle, yet intriguing structural differences. At the ruthenium site a slight elongation of the Ru−C(CO) bond by 0.03 Å contrasts with a larger shortening of the Ru−C(vinyl) bond of about 0.06 Å. While there are no significant structural differences at the vinyl group itself, we note a distinct lengthening of the Fe−C bonds and a concomitant increase of the distances between the Fe atom and the centroids of the cyclopentadienyl rings (Fe−$Cp_{centroid}$) by about 0.05 Å. This is augmented by an inclination of the cyclopentadienyl rings by 12.9° in the solvent-free crystal and by 8.1° in the monosolvate and by a distinct distortion of both Cp rings toward

Chart 2

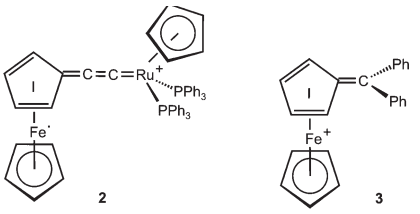

allyl-ene type structures with shorter bonds to the carbon atoms at the less open side. The bonds between the Fe atom and the vinyl-substituted carbon C(22) are particularly long at 2.172(4) or 2.145(4) Å. Similarly long Fe−C_{ipso} bonds of 2.160 and 2.175 Å have been reported for complex **2** and for the diphenylferrocenylcarbenium cation **3**, where a large contribution of the fulvalenyl structure is assumed (Chart 2).[95]

The availability of both **1** and $\mathbf{1}^{\bullet+}\mathbf{PF_6^-}$ as pure, crystalline materials enables us further to compare their IR, UV/vis/NIR, ESR, and Moessbauer spectra in the solid state. Spectral comparison of the solid-state IR spectra indicated a general blue shift of the charge-sensitive IR labels on the ferrocene and the ruthenium sites upon one-electron oxidation, as it was observed in fluid solution. Strikingly, the charge density loss suffered by the ruthenium atom seems to be lower, while that on the ferrocene site is seemingly higher when compared to the fluid solution data. Thus, $\tilde{\nu}$(CO) increased by only 10 cm^{-1} (1902 → 1912 cm^{-1}), while $\tilde{\nu}$(CH) changed by 24 cm^{-1} (3092 → 3116 cm^{-1}) as compared to shifts of 24 ($\tilde{\nu}$(CO)) and 14 cm^{-1} ($\tilde{\nu}$ (CH)) in CH_2Cl_2 or the 1,2-$C_2H_4Cl_2$/NBu_4PF_6 electrolyte. Unfortunately, absorptions of the PF_6^- counterion strongly overlap with those of the perpendicular C−H bend, the position of which is also diagnostic of the ferrocene oxidation state.[61] We also note the appearance of a rather intense absorption at 555 cm^{-1}, which has no counterpart in neutral **1**. UV/vis/NIR spectra of the solid samples were measured on ground powdery samples on an adhesive tape in the transmission mode. Under these conditions neutral **1** exhibits a peak at 300 nm (33 333 cm^{-1}) along with unresolved shoulders that could be deconvoluted into absorptions at 387 nm (25 850 cm^{-1}), 474 nm (21 100 cm^{-1}), and 561 nm (17 800 cm^{-1}). Oxidized $\mathbf{1}^{\bullet+}\mathbf{PF_6^-}$ displayed bands at 391 nm (25 540 cm^{-1}), 550 nm (18 200 cm^{-1}), 1325 nm (7550 cm^{-1}), and 2272 nm (4400 cm^{-1}), in good match with the solution data. The ESR spectrum of a sample of pure $\mathbf{1}^{\bullet+}\mathbf{PF_6^-}$ dissolved in CH_2Cl_2 was also identical to that of the electrogenerated one.

Moessbauer spectra of solid **1** and $\mathbf{1}^{\bullet+}\mathbf{PF_6^-}$ confirm their purities. There is not much change in the isotropic shift from 0.520(1) mm·s^{-1} in **1** to 0.530(1) mm·s^{-1} in $\mathbf{1}^{\bullet+}\mathbf{PF_6^-}$ but a significant reduction in the quadrupole splitting constant from 2.33(1) mm·s^{-1} in **1** to 0.92(1) mm·s^{-1} in $\mathbf{1}^{\bullet+}\mathbf{PF_6^-}$ (Figure 9). This is also in line with an only partial ferrocenium character of the $\mathbf{1}^{\bullet+}$ cation (*vide infra*).

Quantum Chemical Calculations. With the molecular structures and the spectroscopic properties of **1** in different oxidation states at hand it was of interest to gather additional information on its electronic structure and on how it is affected by oxidation. Other issues of interest include charge and spin delocalization in the radical cation, charge density differences upon one-electron oxidation, and the origin of

(95) Behrens, U. *J. Organomet. Chem.* **1979**, *182*, 89–98.

the low-energy bands in $\mathbf{1}^{\bullet+}\mathbf{PF_6}^-$. These were addressed by quantum chemical calculations. In order to separate steric and electronic effects in the geometry optimization and to reduce computational time to a reasonable limit, the calculations were run on simplified model complexes with PH_3 ($\mathbf{1}^{\mathbf{H}}$, $\mathbf{1}^{\mathbf{H}\bullet+}$) or PMe_3 ($\mathbf{1}^{\mathbf{Me}}$, $\mathbf{1}^{\mathbf{Me}\bullet+}$, and $\mathbf{1}^{\mathbf{Me}\,2+}$) instead of P^iPr_3 ligands. The DFT calculations reproduce the experimental structures of both **1** and $\mathbf{1}^{\bullet+}$ and the structural changes upon one-electron oxidation reasonably well, as can be inferred from the comparison of calculated and experimental data in Table 3 and the graphical representations of the optimized structures in Figure S11 of the Supporting Information. Specifically, they predict a slight elongation of the Ru−P, Ru−C(CO), and the vinyl C=C bonds upon oxidation and some larger contraction of the Ru−C(vinyl) bond, in agreement with our crystallographic data. They also produce the experimentally observed elongation of the Fe−ring distances and the structural distortion toward a bent metallocene structure at the ferrocene site upon oxidation. A comparison of experimental structure data of $\mathbf{1}/\mathbf{1}^{\bullet+}$ and the calculated ones for the pairs of $1^{\mathbf{Me}}/\mathbf{1}^{\mathbf{Me}\bullet+}$ and the $\mathbf{1}^{\mathbf{H}}/\mathbf{1}^{\mathbf{H}\bullet+}$ model complexes as provided in Table 3 clearly shows that this distortion is largely independent of the PR_3 ligands on ruthenium. Irrespective of the model complex, ring tilting is about 5−6° larger for the oxidized form than it is for the neutral.

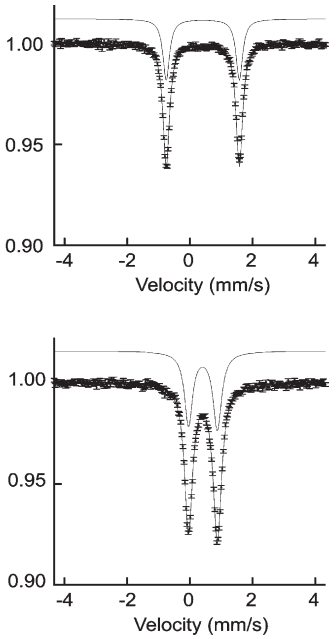

Figure 9. Moessbauer spectra of powdered solid **1** (top) and $\mathbf{1}^{\bullet+}\mathbf{PF_6}^-$ (bottom) at $T = 25$ K. Isomeric shifts are relative to the source with $\delta = -0.11$ with respect to α-Fe.

Figures 10 and 11 list all orbitals of $\mathbf{1}^{\mathbf{Me}}$ and $\mathbf{1}^{\mathbf{Me}\bullet+}$ that are involved in the anodic electrochemistry and in the optical transitions. DFT calculations indicate that the HOMO of neutral **1** is delocalized across the entire metal-organic π-system with contributions of 29% from the iron atom, 5% and 12% from the unsubstituted and substituted cyclo-

Table 3. Structural Comparison of DFT-Optimized Structures of Model Complexes $1^{\mathbf{Me}}/\mathbf{1}^{\mathbf{Me}\bullet+}$ and of the Experimental Structures in the Solvent-Free Crystals

	neutral			radical cation		
	1 (exptl)	$\mathbf{1}^{\mathbf{Me}}$ (calcd)	$\mathbf{1}^{\mathbf{H}}$ (calcd)	$\mathbf{1}^{\bullet+}$ (exptl)	$\mathbf{1}^{\mathbf{Me}\bullet+}$ (calcd)	$\mathbf{1}^{\mathbf{H}\bullet+}$ (calcd)
Ru−Cl	2.4380(5)	2.424	2.403	2.4305(10)	2.410	2.390
Ru−P	2.4107(5), 2.3950(5)	2.352, 2.356	2.323, 2.323	2.4261(10), 2.4252(10)	2.372, 2.375	2.339, 2.375
Ru−C(CO)	1.820(2)	1.810	1.830	1.851(4)	1.829	1.848
Ru−C(vinyl)	1.996(2)	2.016	2.028	1.955(4)	1.958	1.980
C=C	1.339(3)	1.343	1.341	1.354(5)	1.367	1.356
=C−C(Fc)	1.463(3)	1.464	1.463	1.458(5)	1.431	1.441
$Fe-Cp_{sub,centr.}$	1.653	1.662	1.654	1.699	1.688	1.729
$Fe-Cp_{unsub,centr.}$	1.654	1.666	1.658	1.712	1.727	1.731
Ru−C=C	134.8(2)	122.9	122.9	134.70(3)	124.2	124.0
C=C−C	123.6(2)	124.7	124.4	123.40(3)	123.4	124.0
Ru−C=C−C	179.4(2)	173.8	179.7	179.7(3)	171.4	179.7
interplanar angle (Cp)[a]	1.4	1.7	0.1	12.9	8.0	5.1

[a] Angle between the best cyclopentadienyl ring planes.

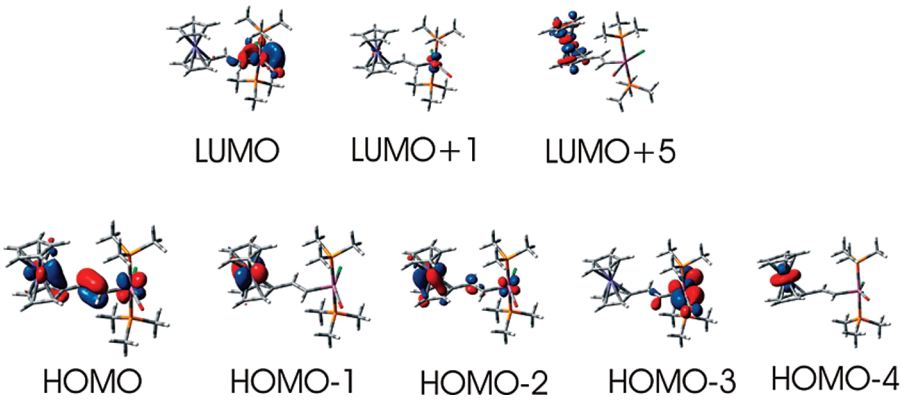

Figure 10. Frontier MOs involved in calculated excitations of $\mathbf{1}^{\mathbf{Me}}$.

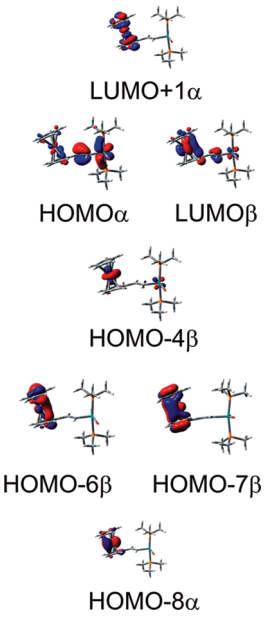

Figure 11. Frontier MOs involved in calculated excitations of $\mathbf{1}^{\mathbf{Me}\bullet+}$.

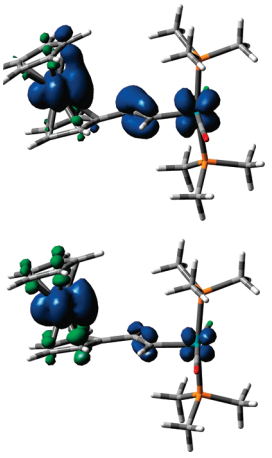

Figure 12. DFT-calculated spin densities for $\mathbf{1}^{\mathbf{Me}\bullet+}$ using the BPW91 (top) or PBE0 (bottom) functional.

pentadienyl ligands, 30% from the vinyl group, and 24% from the $RuCl(CO)(PMe_3)_2$ moiety. One-electron oxidation removes electron density from essentially the delocalized HOMO, as can be seen from the spin density plots provided in Figure 12. The calculated shifts of ν(CO) and ν(C=C) upon oxidation indicate some loss of charge density from the vinyl ruthenium site and qualitatively agree with our experimental observations (Table 4). The calculations, however, seem to overestimate somewhat the ruthenium contribution to the oxidation process. The appearance of IR bands at 555 cm^{-1} and in the 1490 cm^{-1} region of $\mathbf{1}^{\mathbf{Me}\bullet+}$ is also well reproduced by calculations. These bands are due to combinations of Ru−C stretching and Ru−C−C bending modes (550 cm^{-1}) and of C=C stretching and C−C−H bending modes (1490 cm^{-1}).

DFT-calculated spin densities of $\mathbf{1}^{\mathbf{Me}\bullet+}$ are graphically represented in Figure 12. BPW91 calculations give 0.714 on iron (0.655 for the total ferrocene fragment), 0.168 on ruthenium (0.178 for the entire $RuCl(CO)(PMe_3)_2$ entity), and 0.167 for the vinyl group and confirm spin delocalization across the entire $Ru-CH=CH-Fc^{\bullet+}$ system. PBE0-calculated spin densities are 1.083, 0.048, and 0.053 on iron, ruthenium, and the vinyl group, respectively.

TD-DFT calculations on $\mathbf{1}^{\mathbf{Me}\,n+}$ reproduce the experimentally observed pattern of electronic transitions for every accessible oxidation state (n = 0, 1, 2) but grossly underestimate the oscillator strengths of the low-energy absorptions of the radical cation (see Figure S12 of the Supporting Information). On the basis of these calculations it is possible to assign the relevant absorptions (see Figures 10, 11, 13 and Table 5). Specifically, the low-energy bands calculated for $\mathbf{1}^{\mathbf{Me}\bullet+}$ are essentially associated with a redistribution of electron density within the ferrocene nucleus with both d→d and cyclopentadienyl intraligand contributions (Figure 13). The calculated charge transfer to the vinyl ruthenium subunit is only 5.1% or 2.5% for the 2150 and 1370 nm transitions, respectively. The same applies to the d^2A band at a calculated wavelength of 579 nm. Only the e^2A and f^2A bands at calculated wavelengths of 546 at 539 nm receive a significant charge-transfer component from the vinyl ruthenium to the ferrocenyl subunit (Figure 13) but also incorporate additional contributions from intraferrocenyl excitations.

Further oxidation to $\mathbf{1}^{\mathbf{2}+}$ generates a spectrum with only one prominent band at 418 nm. According to our calculations it is dominated by the ferrocene HOMO−4→LUMO transition and is associated with some charge transfer from the ferrocene to the vinyl ruthenium subunit. Lower energy transitions that appear as shoulders in the experimental spectrum originate from more delocalized MOs HOMO and HOMO−1 (see Figure S13 of the Supporting Information).

Discussion

Complex **1** features conjoined electron-rich and easily oxidizable ferrocene and (vinyl)ruthenium[92] subunits. Given that the $Ru(vinyl)Cl(CO)(P^iPr_3)_2$ moiety resembles a dialkylamino substituent in terms of its electron-releasing properties,[38,42,96] the low first oxidation potential of complex **1**, −235 mV, is readily interpreted as that of an electron-rich ferrocene derivative. It compares well to that of −255 mV for di(*p*-tolyl)aminoferrocene[97] and is considerably lower than those of +22 or +5 mV reported for vinylferrocene[98] or α-methylstyrylferrocene, $CpFeC_5H_4CMe=CHPh$.[99] The role of the (vinyl)ruthenium moiety can, however, not be reduced to a mere inductive one. Resonance within the fully conjugated ferrocenyl−vinyl−ruthenium system leads to a situation where the two unlike redox sites share the positive charge in $\mathbf{1}^{\bullet+}$, albeit to a different degree. The electronic structure of $\mathbf{1}^{\bullet+}$ may thus be approximated as $Fc^{\delta+}-\{CH=CH-RuCl(CO)(P^iPr_3)_2\}^{(1-\delta)+}$ where δ represents the fraction of positive charge that resides on the ferrocene part of this molecule. $\mathbf{1}^{\bullet+}$ thus resembles an unsymmetrically substituted biferrocenium cation, $[Cp^RFe-C_5H_4-C_5H_4FeCp^{R'}]^{\bullet+}$.

(96) Maurer, J.; Sarkar, B.; Kaim, W.; Winter, R. F.; Záliš, S. *Chem.—Eur. J.* **2007**, *13*, 10257–10272.
(97) Mendiratta, A.; Barlow, S.; Day, M. W.; Marder, S. R. *Organometallics* **1999**, *18*, 454–456.
(98) Scholl, H.; Sochaj, K. *Electrochim. Acta* **1991**, *36*, 689–694.
(99) Silva, M. E. N. R. A.; Pombeiro, A. J. L.; Silva, F. d.; R., J. J.; Herrmann, R.; Deus, N.; Bozak, R. E. *J. Organomet. Chem.* **1994**, *480*, 75–90.

Table 4. Comparison of Calculated and Experimental IR Frequencies for 1, $1^{\bullet+}$, and 1^{2+} and Its $1^{Me\,n+}$ Model Complexes (energies in cm^{-1})

	neutral			radical cation			dication		
assignment	**1**	$\mathbf{1^{Me}}$ PBE0[a]	$\mathbf{1^{Me}}$ BPW91	$\mathbf{1^{\bullet+}}$	$\mathbf{1^{Me\,\bullet+}}$ PBE0[a]	$\mathbf{1^{Me\,\bullet+}}$ BPW91	$\mathbf{1^{2+}}$	$\mathbf{1^{Me\,2+}}$ PBE0[a]	$\mathbf{1^{Me\,2+}}$ BPW91
ν(Ru−C) + δ(Ru−C−C)		573 (w)	562 (w)	555	564	548		541	563
ν(C═C) + δ(C−C−H)	1571	1539	1543	1498, 1485	1461	1481	[b]	1099	1195
ν(CO)	1908	1908	1921	1932	1943	1958	2004	2009	2009

[a] PBE0 calculated values scaled by a factor of 0.9385. [b] Not detected because of background absorption from the electrolyte.

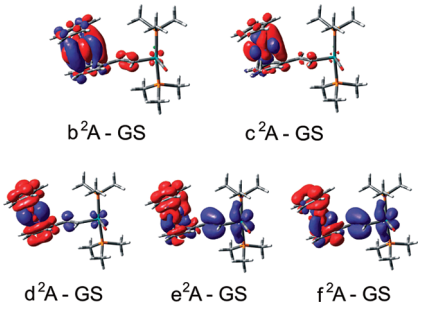

Figure 13. Electron density redistribution in the course of lowest lying excitations within $\mathbf{1^{Me\,\bullet+}}$. Blue and red areas indicate diminishing and increasing electron densities, respectively.

The crystallographically determined structures of **1** and $\mathbf{1^{\bullet+}}$ indicate the presence of an almost ferrocenium-type site in $\mathbf{1^{\bullet+}}$ but also some charge delocalization onto the vinyl ruthenium entity. Thus, the average distance of the iron atom to the centroids of the cyclopentadienyl rings increases upon oxidation from 1.653 Å in **1** to 1.700 Å in $\mathbf{1^{\bullet+}}$. These are essentially the values of the parent neutral ferrocene[100] and ferrocenium[101] ion, respectively. On the other hand, there is a slight but statistically meaningful elongation of the Ru−P and Ru−C(CO) bond lengths, which indicates some loss of electron density from the ruthenium site and decreasing back-donation to the π-accepting co-ligands. Similar situations have been observed for valence-trapped biferrocenium cations[66,102] and the radical cation of a ruthenium ferrocenylacetylide[69] that belongs to class II of mixed-valent compounds according to the Robin and Day classification scheme.[3] Moreover, one-electron oxidation of **1** results in an appreciable ring tilt of about 8−13°. In contrast, the Cp rings are nearly coplanar in neutral **1** with tilt angles in the range 1−3°. Geometry optimizations of the gas-phase structures of the $\mathbf{1^{H\,\bullet+}}$ and $\mathbf{1^{Me\,\bullet+}}$ model complex cations predict such ring tilting, irrespective of the electronic and steric properties of the phosphine co-ligands. We therefore conclude that this structural distortion is of electronic origin and not imposed by crystal-packing forces. Ring tilting increases the overlap between iron- and cyclopentadienyl-based fragment orbitals and aids in charge delocalization.[103] Correlations between ring tilting and intramolecular electron-transfer rates have been noted for biferrocenium cations.[66,104] Ring tilting has also the effect of lifting the degeneracy of the e_g δ orbitals; that is, it stabilizes the $d_{x^2-y^2}$ with respect to the d_{xy} orbital.[103−105] This is seen in the electronic spectrum of $\mathbf{1^{\bullet+}}$ (*vide infra*). The likewise observed shortening of the Ru−C(vinyl) bond upon oxidation points to some contribution of the fulvalenyl-type canonical structures II and III in Chart 3 to the electronic description of $\mathbf{1^{\bullet+}}$, as proposed for ferrocenylacetylide iron and ruthenium complexes.[69,106]

One diagnostic for estimating the fractions of positive charge δ on the ferrocenyl unit and $1-\delta$ on the (vinyl) ruthenium site is the oxidation-induced shift of $\tilde{\nu}$(CH, Cp) and $\tilde{\nu}$(Ru−CO). These parameters present charge-sensitive IR labels at the ferrocene and the ruthenium sites. With 24 cm^{-1}, $\Delta\tilde{\nu}$(CO) amounts to about 40% of the 65 cm^{-1} shift observed for the 0/+ couple of the comparable styryl complex Ru(CH═CHPh)Cl(CO)(P^iPr_3)$_2$.[92] In the same vein, the shift of the cyclopentadienyl ν(CH) on ferrocene upon oxidation is smaller than that reported for the ferrocene/ferrocenium couple.[94] An estimate of the overall proportion of the positive charge residing on the $Fc^{\delta+}$ site of $\mathbf{1^{\bullet+}}$ is provided by fully oxidized $\mathbf{1^{2+}}$. Identifying the observed total shift of 26 cm^{-1} as that corresponding to the removal of one full electron from the ferrocene, the observed 16 cm^{-1} shift upon the first oxidation yields a δ value of about 60%, in agreement with the $1-\delta$ value derived from $\Delta\tilde{\nu}$(CO). Monooxidized $\mathbf{1^{\bullet+}}$ thus constitutes an almost delocalized heterobimetallic mixed-valent system. These data, however, pertain to the fluid solution. IR measurements indicate a less symmetric charge distribution in the solid state. Under these conditions, $\Delta\tilde{\nu}$(CO) of $\mathbf{1^{\bullet+}}$ amounts to just 10 cm^{-1}, while $\Delta\tilde{\nu}$(CH, Fc) increases to 24 cm^{-1}. This is highly reminiscent of the situation in mixed-valent biferrocenium radical cations, where the charge distribution and charge-transfer dynamics depend profoundly on the counterions, the structural organization and relative orientations of the cations and the counterions in the crystal, the hydrogen-bonding network interconnecting them, and lattice dynamics.[62,67,102,107−111] Larger charge localization at the ferrocenyl subunit when compared to the fluid solution arises most probably from the positioning of the PF_6^- counterion. In the solid state, CH···F hydrogen-bonding interactions hold the

(100) Seiler, P.; Dunitz, J. D. *Acta Crystallogr. B 35*, 1068-1074.
(101) Mammano, N. J.; Zalkin, A.; Landers, A.; Rheingold, A. L. *Inorg. Chem.* **1977**, *16*, 297–300.
(102) Dong, T.-Y.; Hendrickson, D. N.; Pierpont, C. G.; Moore, M. F. *J. Am. Chem. Soc.* **1986**, *108*, 963–971.
(103) Dong, T.-Y.; Lee, S.-H. *J. Organomet. Chem.* **1995**, *487*, 77–88.
(104) Dong, T.-Y.; Huang, C.-S.; Chang, C.-K.; Wen, Y.-S.; Lee, S.-L.; Chen, J.-A.; Yeh, W.-Y.; Yeh, A. *J. Am. Chem. Soc.* **1993**, *115*, 6357–6368.
(105) Albright, T. A. *Tetrahedron* **1982**, *38*, 1339–1388.
(106) Sato, M.; Kawata, Y.; Shintate, H.; Habata, Y.; Akabori, S.; Unoura, K. *Organometallics* **1997**, *16*, 1693–1701.
(107) Hendrickson, D. N.; Oh, S. M.; Dong, T.-Y.; Kambara, T.; Cohn, M. J.; Moore, M. F. *Commun. Inorg. Chem.* **1985**, *4*, 329–349.
(108) Dong, T.-Y.; Kambara, T.; Hendrickson, D. N. *J. Am. Chem. Soc.* **1986**, *108*, 5857–5865.
(109) Dong, T.-Y.; Kambara, T.; Hendrickson, D. N. *J. Am. Chem. Soc.* **1986**, *108*, 4423–4432.
(110) Kai, M.; Katada, M.; Sano, H. *Chem. Lett.* **1989**, *18*, 1473–1476.
(111) Kambara, T.; Hendrickson, D. N.; Dong, T.-Y.; Cohn, M. J. *J. Am. Chem. Soc.* **1987**, *86*, 2362–2374.

Table 5. TD-DFT (PBE0/CPCM) Selected Calculated Excitation Energies (eV) for 1^{Me}, $1^{Me\bullet+}$, and $1^{Me\,2+}$ Calculated for CH_2Cl_2 Solution

n	state	main contributing excitations (%)	transition energy eV (nm)	osc str	expt (nm)	molar absorpt (M^{-1} cm^{-1})
0	b^1A	99 (HOMO−1 → LUMO + 5)	2.21 (562)	0.004	529	360
	c^1A	99 (HOMO → LUMO)	2.37 (522)	0.006	455	525
	e^1A	94 (HOMO−3 → LUMO)	3.21 (387)	0.028	381	2340
	f^1A	96 (HOMO−4 → LUMO)	4.48 (278)	0.062	300	17 000
	h^1A	mixed	4.55 (272)	0.331		
1	b^2A	30 (HOMO−6β → LUMOβ)	0.53 (2315)	0.0	2150	710
		55 (HOMO−7β → LUMOβ)				
	c^2A	70 (HOMO−4β → LUMOβ)	0.97 (1275)	0.003	1371	2700
	d^2A	36 (HOMO-8α → LUMO + 1α)	2.14 (579)	0.053	556	5000
	e^2A	40 (HOMOα → LUMO + 1α)	2.27 (546)	0.094	504	3320
	f^2A	40 (HOMOα → LUMO + 1α)	2.30 (539)	0.073		
	g^2A	mixed	3.20 (387)	0.146	415	3150
h^2A	mixed	3.95 (314)	0.088	278	11 500	
	i^2A	60 (HOMO−5α → LUMO + 1α	4.03 (308)	0.082		
2	b^1A	80 (HOMO → LUMO)	2.41 (515)	0.059	540	sh
	c^1A	78 (HOMO-1 → LUMO)	2.54 (488)	0.012		
	e^1A	mixed	2.84 (434)	0.063	418	∼13 500
	f^1A	95 (HOMO−1 → LUMO)	3.32 (373)	0.035		
	h^1A	60 (HOMO−4 → LUMO)	3.38 (367)	0.281		

Chart 3. Resonance Structures of $1^{\bullet+}$

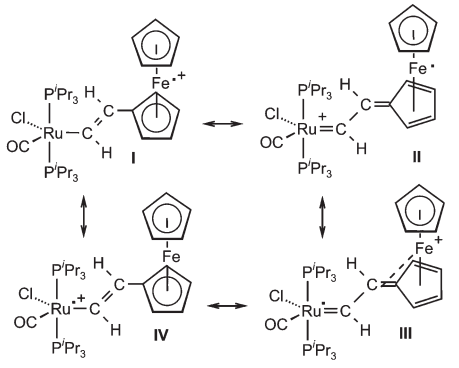

Chart 4

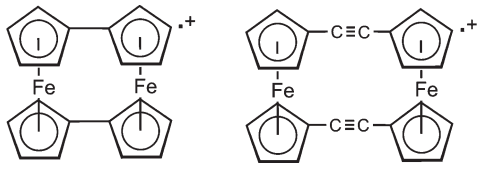

PF_6^- anion close to the ferrocenyl entity and reduce its mobility.

In keeping with the idea of an only partial ferrocenium character of $\mathbf{1}^{\bullet+}$, its ESR and Moessbauer spectra differ substantially from those of classical ferrocenium ions. Contrary to most simple ferrocenium systems, $\mathbf{1}^{\bullet+}$ is ESR active at 110 K and displays a rather small *g*-tensor anisotropy of 0.96. In addition, the Moessbauer quadrupole splitting ΔE_Q of 0.92 mm/s of solid $\mathbf{1}^{\bullet+}$ is unusually large. This is reminiscent of valence-delocalized mixed-valent biferrocenium radical cations or of ferrocenium cations with substantial charge delocalization onto conjugated ring substituents[65] and of the related ethynyl-bridged $[Cp(PPh_3)_2Ru{-}C{\equiv}C{-}Fc]^{\bullet+}$[69] and $[1,1'\text{-}\{Cp(PPh_3)_2Ru{-}C{\equiv}C{-}C_5H_4\}_2Fe]^{\bullet+}$[72] radical cations, for which ΔE_Q values of 0.77 or 0.952 mm/s have been measured. Hendrickson et al. have observed a linear increase of ΔE_Q values for ferrocenium and biferrocenium ions over the continuum regime between valence-averaged class III ($\delta = 0.5$) and valence-trapped class II ($\delta \approx 1$) systems.[61] Taking the values of ca. 0.15 mm/s for ordinary ferrocenium ions[112−114] in valence-trapped systems and of ca. 1.6 for the genuine class III bis(fulvalenyl)diiron and [2,2]ferrocenophane-1,13-diyne radical cations[61] ($\delta = 0.5$, Chart 4) allows for a rough estimate of $\delta \approx 0.8$ for $\mathbf{1}^{\bullet+}$ in the solid state as compared with $\delta = 0.6$ in solution.

Low-energy absorption bands in mixed-valent complexes are commonly identified as arising from intervalence charge transfer, i.e., the transfer of charge from the (formally) reduced to the (formally) oxidized site across the intervening bridge. While $\mathbf{1}^{\bullet+}$ features two bands that would be likely candidates of such absorptions, our quantum chemical calculations provide us with very little evidence that this is really the case here. Both underlying transitions are dominantly iron-centered d−d type transitions. Thus, the band at 2150 nm arises mainly from a transition between the two nondegenerate δ orbitals, while the 1370 nm band corresponds to a transition from the iron-centered d_{z^2} to the higher lying δ orbital. Both receive only little admixture from charge transfer to the vinyl ruthenium unit. Such a situation is somewhat reminiscent of half-sandwich $CpFeL_2$-type systems, which also feature d−d type transitions in their oxidized states.[7] The availability of pure $\mathbf{1}^{\bullet+}\mathbf{PF_6}^-$ allowed us to record its UV/vis/NIR spectrum in media of widely different dielectric strength and Onsager solvent polarity functions without the restrictions imposed by the conditions of spectroelectrochemistry. These studies revealed an only weak and nonsystematic solvatochromism of every band. While such behavior could in principle arise from opposing solvent effects on the free energy difference ΔG^0 between the different valence-localized states and the outer reorganization energy λ_o,[115] it probably attests to the delocalized electronic structure of $\mathbf{1}^{\bullet+}$.[72]

Further insight into the degree of electron delocalization in $\mathbf{1}^{\bullet+}$ and its medium dependence can be gathered from the comparison of the experimental and the theoretical bandwidth (eq 6) of the merged e^2A and f^2A HOMOα → LUMO

(112) Wertheim, G. K.; Herber, R. H. *J. Chem. Phys.* **1963**, *38*, 2106–2111.
(113) Collins, R. L. *J. Chem. Phys.* **1965**, *42*, 1072–1075.
(114) Moore, M. F.; Wilson, S. R.; Cohn, M. J.; Dong, T. Y.; Mueller-Westerhoff, U. T.; Hendrickson, D. N. *Inorg. Chem.* **1985**, *24*, 4559–4565.
(115) Heckmann, A.; Lambert, C. *J. Am. Chem. Soc.* **2007**, *129*, 5515–5527.

$+1\alpha$ transitions that have been identified as being associated with charge transfer from the vinyl ruthenium to the ferrocene site admixed with intraligand transitions of ferrocene (Table 5, Figures 11 and 13). The Γ parameter as defined in eq 7 provides another measure of electron delocalization in mixed-valent systems, assuming values of 0 for valence localized, of $0 \leq \Gamma \leq 0.5$ for class II systems, of ca. 0.5 for class II/III borderline systems, and of >0.5 for intrinsically delocalized systems of class III.[52]

$$\Delta\tilde{\nu}_{1/2,\,\mathrm{calcd}} = (2310\tilde{\nu}_{\max})^{1/2} \quad (6)$$

$$\Gamma = 1 - (\Delta\tilde{\nu}_{1/2,\,\mathrm{exp}}/\Delta\tilde{\nu}_{1/2,\,\mathrm{calcd}}) \quad (7)$$

In the present case, analysis was complicated by the overlap of the merged, broader IVCT band with the ferrocene localized HOMO$-8\alpha \rightarrow$ LUMO$+1\alpha$ band at somewhat lower energies (Table 5 and Figure 11). Although very satisfactory fits could be obtained over the entire UV/vis region by invoking five separate transitions, the derived parameter sets have to be regarded with the usual caveats of such deconvolution procedures. Nevertheless, data acquired in solvents as they are compiled in Table S3 of the Supporting Information give the intuitively reasonable result of increasing electron delocalization with decreasing solvent polarity and decreasing ability of the solvent to stabilize charge accumulation by solvation. DMF ($\Gamma = 0.28$) and toluene ($\Gamma = 0.56$) constitute the extremes in the studied range of solvents. In any event these results provide further evidence for the positioning of $\mathbf{1}^{\bullet+}\mathbf{PF_6}^-$ close to or at the class II/III borderline, at least in less polar media.

No reasonable results were, however, obtained when applying the equations routinely used for the interpretation of IVCT bands in mixed-valent systems to the merged e^2A and f^2A band of $\mathbf{1}^{\bullet+}$. The intrinsic energy difference ΔG^0 between the Fc^+-(CH=CH)RuCl(CO)(P^iPr_3)$_2$ and the Fc-{(CH=CH)RuCl(CO)(P^iPr_3)$_2$}$^+$ valence tautomers of eq 3 can be approximated as 275 mV (2220 cm^{-1}) from the redox potentials of α-methylstyrylferrocene ($+$ 5 mV) and of Ru(CH=CHPh)Cl(CO)(P^iPr_3)$_2$ ($+280$ mV). Since the IVCT band energy amounts to 19840 cm^{-1}, one obtains an unrealistically high λ value of 17620 cm^{-1}. Likewise, the V_{ab} value of 1700 cm^{-1} according to eq 1 and the resulting delocalization parameter α ($\alpha = V_{ab}/\tilde{\nu}_{max}$) of 0.086 seem much too low.

The IR spectroscopic changes upon the further oxidation to $\mathbf{1}^{2+}$ indicate that the second oxidation also involves *both* redox sites with, however, higher contributions of the (vinyl) ruthenium site. Thus, $\Delta\tilde{\nu}$(CO) amounts to 72 cm^{-1}, while $\Delta\tilde{\nu}$(CH, Fc) is 10 cm^{-1}.

Conclusions

In summary, the ruthenium-substituted vinylferrocene **1** constitutes a mélange of two intimately coupled, electron-rich redox-active subunits. Oxidation involves a frontier orbital that is delocalized over both its redox-active constituents but more biased on the ferrocene site. The results from IR, ESR, and Moessbauer spectroscopies and the comparison of three different crystallographically determined structures of **1** and two of $\mathbf{1}^{\bullet+}$ as well as the quantum chemical calculations agree with this view. Our results also indicate a profound matrix effect on the charge distribution with a more symmetrical, delocalized one in low-polarity solvents such as toluene, CH_2Cl_2, and 1,2-$C_2H_4Cl_2$/NBu_4PF_6 solutions and a more localized one in polar DMF or in the solid. Estimates derived from the $\Delta\tilde{\nu}$(CO) of the ruthenium carbonyl and the $\Delta\tilde{\nu}$(CH) of the ferrocene cyclopentadienyl rings in 1,2-$C_2H_4Cl_2$/NBu_4PF_6 solution place 60% of the positive charge on the ferrocenium site, while the value derived from $\Delta\tilde{\nu}$(CO) and ΔE_Q measured on solid samples provide an estimate of ca. 80%. The higher degree of charge localization in the solid is probably a result of CH$\cdots$F hydrogen-bonding interactions that lock the PF_6^- counterion close to the ferrocenium site.

Despite the mixed-valent character of $\mathbf{1}^{\bullet+}$, the observed low-energy bands seem to arise from transitions that are largely confined to the $Fc^{\delta+}$ subunit with only minor charge transfer to the vinyl ruthenium site. They are probably best described as iron-based d$-$d type transitions. A rather intense band at 504 nm is, however, identified as receiving major contributions from (vinyl)ruthenium$^{(1-\delta)+}\rightarrow Fc^{\delta+}$ charge transfer. Our results also underpin that Ru(vinyl)Cl(CO)(P^iPr_3)$_2$ entities rival or even surpass $Cp^R(PR_3)_2Ru-C\equiv C-$ (Cp^R = Cp, Cp*; $(PR_3)_2$ = dppe, $(PPh_3)_2$, $(PEt_3)_2$) or $Cl(L_2)_2Ru-C\equiv C-$ (L_2 = chelating diphosphine) ones with respect to providing charge delocalization in ferrocenyl$-$bridge$-${Ru} assemblies.

Experimental Section

General Conditions. All preparations were carried out using standard Schlenk techniques. Chromatographic separations were carried out using silica gel 60 (Merck, 230$-$400 mesh ASTM). Tetrahydrofuran was distilled over sodium benzophenone ketyl. Dichloromethane was freshly distilled from CaH_2 handled under nitrogen. Other solvents were of reagent grade and were used without prior purification. RuClH(CO)(P^iPr_3)$_2$ was prepared according to the literature procedure.[81] All other chemicals were purchased from the Aldrich Chemical Co. The NMR spectra were recorded on a Bruker AV300 spectrometer. Chemical shifts are reported in δ (ppm) using residual $CHCl_3$ (^{1}H δ 7.26 ppm) and $CDHCl_2$ (^{1}H δ 5.32 ppm) as the reference. Mass spectra were recorded using EI methods on a Finnigan MAT 710A spectrometer. Microanalyses were determined by Analytical Services of the University of Regensburg. UV/vis spectra were obtained on an Omega 20 spectrometer from Bruins Instruments in HELMA quartz cuvettes whith 1 cm optical path lengths. The ESR equipment consisted of a Bruker ESP 3000 spectrometer or a Bruker EMX setup equipped with a HP 5350 B frequency counter, a Bruker ER035 M gaussmeter, and a continuous flow cryostat ESR 900 from Oxford Instruments for low-temperature work. Electrochemical work was performed on a BAS CV50 potentiostat in a home-built vacuum-tight one-compartment cell using Pt or glassy carbon disk electrodes from BAS as the working electrode, a platinum spiral as the counter electrode, and a silver spiral as a pseudoreference electrode. Each of the spiral-shaped electrodes was welded to Vycon wire and sealed into a glass tube. Counter and reference electrodes are introduced into the cell by appropriate fittings in the side wall and sealed via a Quickfit screw. The design of the spectroelectrochemical cell follows that of Hartl et al.[116] CH_2Cl_2 and 1,2-$C_2H_4Cl_2$ for electrochemical use were of Burdick & Jackson brand (Fluka) and were distilled from CaH_2, deoxygenated by saturation with argon, and briefly stored over molecular sieves. Potential calibration was performed by adding ferrocene as an internal standard to the analyte solution. The amount of the reference system was adjusted until its peak currents were comparable to those of the analyte. Potentials are given against the ferrocene/ferrocenium couple. **Cautionary Note:** 1,2-Dichloroethane (DCE) is

(116) Krejcik, M.; Danek, M.; Hartl, F. *J. Electroanal. Chem.* **1991**, *317*, 179–187.

Table 6. Crystal Data and Structure Refinement for the Different Crystal Structure Determinations of 1 and $1^{\bullet+}$

	1	**1**×$CHCl_3$ (green polymorph)	**1**×$CHCl_3$ (purple polymorph)	$\mathbf{1}^{\bullet+}\mathbf{PF_6^-}$	$\mathbf{1}^{\bullet+}\mathbf{PF_6^-}$×$\mathbf{CHCl_3}$
formula	$C_{31}H_{53}ClFeOP_2Ru$	$C_{31}H_{53}ClFeOP_2Ru \times CHCl_3$	$C_{31}H_{53}ClFeOP_2Ru \times CHCl_3$	$C_{31}H_{53}ClF_6FeOP_3RuP$	$C_{31}H_{53}ClF_6FeOP_3RuP \times CHCl_3$
fw	696.04	815.41	815.41	841.01	960.19
cryst syst	triclinic	triclinic	monoclinic	monoclinic	orthorhombic
space group	$P\bar{1}$	$P\bar{1}$	$P2_1/n$	$P2_1/c$	*Pbca*
a [Å]	10.6404(2)	9.8528(3)	8.9227(2)	9.6683(7)	17.0695(2)
b [Å]	12.3258(2)	11.1444(5)	43.0777(6)	24.4298(17)	14.3638(2)
c [Å]	13.2765(3)	17.4601(8)	9.5914(2)	16.1459(11)	33.1562(4)
α [deg]	80.812(2)	102.374(4)	90	90	90
β [deg]	87.993(2)	92.074(3)	92.589(1)	104.503(8)	90
γ [deg]	72.266(2)	98.825(3)	90	90	90
V [Å^3]	1637.04(6)	1845.73(14)	3682.88(12)	3692.1(5)	8129.33(18)
$d_{calcd.}$ [g·cm^{-3}]	1.412	1.467	1.471	1.513	1.569
Z	2	2	4	4	8
F(000)	728	844	1688	1732	3927
μ [mm^{-1}]	1.106	10.125			
cryst dimens [mm]	0.27 × 0.19 × 0.08	0.22 × 0.13 × 0.07	0.17 × 0.06 × 0.02	0.22 × 0.13 × 0.08	0.23 × 0.22 × 0.06
T [K]	123(1)	123(1)	123(1)	123(1)	123(1)
radiation	Mo Kα	Cu Kα	Cu Kα	Mo Kα	Mo Kα
scan range [deg]	3.68 < *θ* < 31.96	2.60 < *θ* < 62.20	4.10 < *θ* < 62.20	2.39 < *θ* < 25.89	2.84 < *θ* < 29.56
reflns measd	28 583	12 833	12 376	31 804	36 950
obsd data	8139 ($I > 2\sigma(I)$)	3870 ($I > 2\sigma(I)$)	4183 ($I > 2\sigma(I)$)	4951 ($I > 2\sigma(I)$)	7949 ($I > 2\sigma(I)$)
data/restraints/params	10 476/0/346	5695/0/382	5440/0/382	7132/0/409	11 289/4/456
goodness-of-fit on F^2	0.983	0.854	0.968	0.885	1.131
R indices ($I > 2\sigma(I)$)	0.0374; 0.0698;	0.0366; 0.0737	0.0341; 0.0736	0.0393; 0.0852	0.0727; 0.1062
R indices (all data)	0.0590; 0.0742	0.0561; 0.0769	0.0491; 0.0787	0.0616; 0.0894	0.1062; 0.1155
max./min. residual electron density [e·Å^{-3}]	−0.428; 1.064	−0.467; 0.768	−0.371; 1.028	−0.439; 1.027	−0.987; 1.435

highly toxic and a suspected carcenogen and should be handled with care.

Quantum Chemical Calculations. The electronic structures were calculated by density functional theory (DFT) methods using the Gaussian 03[117] program package. In order to reduce computational time to a reasonable limit, P^iPr_3 ligands were modeled by PMe_3. Geometry optimizations were performed without any symmetry constraints. Electronic transitions were calculated by the time-dependent DFT (TD DFT) method. Within G03 calculations the quasirelativistic effective core pseudopotentials and the corresponding optimized set of basis functions for Ru and Fe were used.[118] Polarized triple-ζ basis sets (6-311G*,[119] geometry optimization) or polarized double-ζ basis sets cc-pvdz[120] (TD DFT) for the remaining atoms were employed together with the PBE0[121] functional. The solvent was described by the polarizable conductor calculation model (CPCM)[122] in TD DFT calculations. For comparison a vibrational analysis was done also with the "pure" density functional BPW91.[123,124] In order to separate the steric and electronic effects, the geometry optimizations were performed for model complexes with PH_3 and PMe_3 ligands.

Preparation of 1. To a stirring solution of $RuClH(CO)(P^iPr_3)_2$ (105 mg, 0.21 mmol) in dichloromethane (2 mL) was added ethynylferrocene (42 mg, 0.20 mmol) in dichloromethane (3 mL). Briefly after mixing, the solution turned deep red. It was stirred at room temperature for 30 min. After this period the mixture solvent volume was reduced *in vacuo* to approximately 2 mL and then filtered through Celite (rg 521 AW). The solvent was then evaporated, affording a red-brown solid. Recrystallization from hot *n*-hexane yielded ruby-brown rod-shaped X-ray quality crystals of **1** (135 mg, 97%). Alternatively, X-ray quality crystals of **1** were obtained by overnight crystallization from a chloroform/methanol mixture in the freezer. This method afforded a mixture of two types of crystals: purple flat rods and greenish-brown flat prisms (for details see crystallographic section).

^{1}H NMR (600 MHz, $CDCl_3$): *δ* 7.66 (br d, 1H, $^3J_{H-H}$ = 13.3 Hz, Ru-C*H*=CH), 5.54 (dt, 1H, $^3J_{H-H}$ = 13.3 Hz, $^3J_{P-H}$ = 2.0 Hz, RuCH=C*H*), 4.02 (s, 5H, Cp), 4,00 (virtual t, 2H, $^3J_{H-H}$ = 1.7 Hz, $H_{3,4}$-Cp_{sub}), 3.98 (virtual t, 2H, $^3J_{H-H}$ = 1.7 Hz, $H_{2,5}$-Cp_{sub}), 2.81−2.69 (m, 6H, PC*H*$(CH_3)_2$), 1.34−1.25

(117) Frisch, M. J.; Trucks, G.; Schlegel, H. B.; Scuseria, G. E.; Robb, M. A.; Cheeseman, J. R.; Montgomery, J. A., Jr.; Vreven, T.; Kudin, K. N.; Burant, J. C.; Millam, J. M.; Iyengar, S. S.; J. Tomasi, J.; Barone, V.; Mennucci, B.; Cossi, M.; Scalmani, G.; Rega, N.; Petersson, G. A.; Nakatsuji, H.; Hada, M.; Ehara, M.; Toyota, K.; Fukuda, R.; Hasegawa, J.; Ishida, M.; Nakajima, T.; Honda, Y.; Kitao, O.; Nakai, H.; Klene, M.; Li, X.; Knox, J. E.; Hratchian, H. P.; Cross, J. B.; Bakken, V.; Adamo, C.; Jaramillo, J.; Gomperts, R.; Stratmann, R. E.; Yazyev, O.; Austin, A. J.; Cammi, R.; Pomelli, C.; Ochterski, J. W.; Ayala, P. Y.; Morokuma, K.; Voth, G. A.; Salvador, P.; Dannenberg, J. J.; Zakrzewski, V. G.; Dapprich, S.; Daniels, A. D.; Strain, M. C.; Farkas, O.; Malick, D. K.; Rabuck, A. D.; Raghavachari, K.; Foresman, J. B.; Ortiz, J. V.; Cui, Q.; Baboul, A. G.; Clifford, S.; Cioslowski, J.; Stefanov, B. B.; Liu, G.; Liashenko, A.; Piskorz, P.; Komaromi, I.; Martin, R. L.; Fox, D. J.; Keith, T.; Al-Laham, M. A.; Peng, C. Y.; Nanayakkara, A.; Challacombe, M.; Gill, P. M. W.; Johnson, B.; Chen, W.; Wong, W. M.; Gonzalez, C.; Pople, J. A. *Gaussion 03, Revision C.02*; Gaussian, Inc: Wallingford CT, 2004.

(118) Andrae, D.; Haeussermann, U.; Dolg, M.; Stoll, H.; Preuss, H. *Theor. Chim. Acta* **1990**, *77*, 123.

(119) Mc Lean, A. D.; Chandler, G. S. *J. Chem. Phys.* **1980**, *72*, 5639–5648.

(120) Woon, D. E.; Dunning, T. H.Jr. *J. Chem. Phys.* **1993**, *98*, 1358–1371.

(121) Perdew, J. P.; Burke, K.; Enzerhof, M. *Phys. Rev. Lett.* **1996**, *77*, 3865–3868.

(122) Cossi, M.; Rega, N.; Scalmani, G.; Barone, V. *J. Comput. Chem.* **2003**, *24*, 669–681.

(123) Becke, A. D. *Phys. Rev. A* **1988**, *38*, 3098–3100.

(124) Perdew, P. P.; Wang, Y. *Phys. Rev. B* **1992**, *45*, 13244–13249.

(m, 36H, PCH(CH_3)$_2$) ppm. ^{13}C NMR (150 MHz, $CDCl_3$): δ 203.1 (t, $^2J_{C-P}$ = 13.1 Hz, Ru-*C*O), 143.2 (t, $^2J_{C-P}$ = 10.7 Hz, Ru-*C*H=CH), 129.6, (t, $^2J_{C-P}$ = 3.1 Hz, Ru-CH=*C*H), 89.0 (br s, C_1-Cp_{sub}), 68.2 (s, Cp), 66.7 (s, $C_{3,4}$-Cp_{sub}), 64.0 (s, $C_{2,5}$-Cp_{sub}), 24.3 (vt, J = 9.7 Hz, P*C*H(CH_3)$_2$), 19.89, 19.87 (s, PCH(*C*H_3)$_2$) ppm. ^{31}P{^{1}H} NMR (121 MHz, $CDCl_3$): δ 38.58 (s) ppm. EIMS (70 eV, m/z): 695.9 [M^+], 535.8 [$M^+ - C_9H_{21}P^+$], 160.1 [$C_9H_{21}P^+$]. Anal. Calcd for ($C_{31}H_{53}P_2OClFeRu$): C, 53.44; H, 7.67. Found: C, 53.49; H, 7.53.

Preparation of $1^+PF_6^-$. To a vigorously stirred dry mixture of **1** (704 mg, 1.01 mmol) and Fc^+ PF_6^- (334 mg, 1.01 mmol) was added dichloromethane (25 mL). Upon addition of solvent, the reaction mixture became dark violet and was stirred at room temperature for 40 min. The solvent was evaporated to dryness to afford a dark violet solid. This solid was then washed three times with *n*-hexane under ultrasonic agitation, filtered, and dried under vacuum to give a fine violet powder. Crystallization from a *n*-hexane-layered concentrated solution in dichloromethane yielded ruby red plate-like crystals of X-ray quality (807 mg, 95%). Alternatively, dark red plates of X-ray quality were obtained by room-temperature diffusion of *n*-hexane into a saturated chloroform solution of $\mathbf{1}^{\bullet+}\mathbf{PF_6^-}$.

^{1}H NMR (400 MHz, $CDCl_3$): δ 20.45 (br s), 2.91 (br s, C_5H_4, C_5H_5), 1.51 (br s), 1.29 (br s, C*H*(CH_3)$_2$), 1.04 (s, CH(C*H*$_3$)$_2$), 0.94 (s, CH(C*H*$_3$)$_2$). ^{31}P{^{1}H} NMR: δ −151.59 (hept, PF_6^-). ESMS (positive ion, H_2O/CH_3OH + 10 mM NH_4OAc): 720.3 [$M^+ - Cl^- + CH_3COO^-$], 696.3. [M^+] ESMS (negative ion, H_2O/CH_3OH + 10 mM NH_4OAc): 144.9 [PF_6^-]. Anal. Calcd for ($C_{31}H_{53}P_3OClF_6FeRu\times CHCl_3$): C, 40.04; H, 5.67. Found: C, 39.92; H, 5.93.

Crystal Structure Determination. Geometry and intensity data were collected on an Oxford Diffraction Gemini Ultra CCD diffractometer with multilayer optics and with Mo Kα (λ = 0.71073 Å, graphite monochromator) or Cu Kα (λ = 1.54184 Å, graphite monochromator) radiation sources. The structures were solved by direct methods (SIR-97)[125] and refined by full-matrix least-squares on F^2 (SHELXL-97).[126] H atoms were calculated geometrically, and a riding model was applied during the refinement process. A summary of crystallographic data, data collection parameters, and refinement parameters are collected in Table 6. Packing diagrams were generated with the Mercury program.[127] Cif files of the structure determinations have been deposited at the Cambridge Crystallographic Data Centre (CCDC numbers 725430−725434). These data can be obtained free of charge via www.ccdc.cam.-ac.uk/data_request/cif.

Acknowledgment. We thank the Deutsche Forschungsgemeinschaft (grant Wi 1262/7-2) for generous support of this research. K.K. is grateful to the Alexander von Humboldt-Stiftung for a research fellowship at the group of R.F.W., University of Regensburg. The Grant Agency of the Academy of Sciences of the Czech Republic (KAN100400702) and the Ministry of Education of the Czech Republic (Grant COST OC 139) is acknowledged by S.Z. We also thank Teresa Maltry and Philipp Mücke for their studies on the solvent dependence of the UV/vis/NIR bands of $\mathbf{1}^{\bullet+}\mathbf{PF_6^-}$.

Supporting Information Available: ORTEP plots of the structures of the two polymorphs of $\mathbf{1}\times CHCl_3$ and of $\mathbf{1}^{\bullet+}\mathbf{PF_6^-}\times CHCl_3$ along with figures showing the packing in the crystal; lists of bond lengths and angles; figures showing the IR spectroscopic changes during the later stages of the second oxidation of **1** and upon the back-reduction of $\mathbf{1}^{2+}$ to $\mathbf{1}^{\bullet+}$ as well as those observed during the first oxidation of **1** over an extended energy range; figures depicting the optimized structures of the $\mathbf{1}^{Me}$ and $\mathbf{1}^{Me\bullet+}$ model systems and the calculated electronic spectra of $\mathbf{1}^{Me}$ and of $\mathbf{1}^{Me\bullet+}$; plot of the orbitals of $\mathbf{1}^{Me\,2+}$ that are involved in the electronic transitions; table detailing the solvent dependence of the merged d^2A and f^2A bands of $\mathbf{1}^{\bullet+}$ and the derived Γ parameter. This material is available free of charge via the Internet at http://pubs.acs.org.

(125) Altomare, A.; Burla, M. C.; Camalli, M.; Cascarano, G. L.; Giacovazzo, C.; Guagliardi, A.; Moliterni, A. G. G.; Polidori, G.; Spagna, R. *J. Appl. Crystallogr.* **1999**, *32*, 115–119.

(126) Sheldrick, G. M. *SHELXL-97, Program for Crystal Structure Solution and Refinement*; Universität Göttingen, 1997.

(127) *Mercury*, 1.4.2 (Build 2); Cambridge (UK), 2001.